

Self Paced Deep Learning for Weakly Supervised Object Detection

Enver Sangineto[†], Moin Nabi[†], Dubravko Culibrk and Nicu Sebe,

Abstract—In a weakly-supervised scenario object detectors need to be trained using image-level annotation alone. Since bounding-box-level ground truth is not available, most of the solutions proposed so far are based on an iterative, Multiple Instance Learning framework in which the current classifier is used to select the highest-confidence boxes in each image, which are treated as pseudo-ground truth in the next training iteration. However, the errors of an immature classifier can make the process drift, usually introducing many of false positives in the training dataset. To alleviate this problem, we propose in this paper a training protocol based on the self-paced learning paradigm. The main idea is to iteratively select a subset of images and boxes that are the most reliable, and use them for training. While in the past few years similar strategies have been adopted for SVMs and other classifiers, we are the first showing that a self-paced approach can be used with deep-network-based classifiers in an end-to-end training pipeline. The method we propose is built on the fully-supervised Fast-RCNN architecture and can be applied to similar architectures which represent the input image as a bag of boxes. We show state-of-the-art results on Pascal VOC 2007, Pascal VOC 2010 and ILSVRC 2013. On ILSVRC 2013 our results based on a low-capacity AlexNet network outperform even those weakly-supervised approaches which are based on much higher-capacity networks.

Index Terms—Weakly supervised learning, object detection, self-paced learning, curriculum learning, deep learning, training protocol.

1 INTRODUCTION

A well known problem in object detection is the fact that collecting ground truth data (i.e., object-level annotations) for training is usually much more time consuming and expensive than collecting image-level labels for object classification. This problem is exacerbated in the context of the current deep networks, which need to be trained or “fine-tuned” using large amounts of data. Weakly-supervised techniques for object detection (WSD) can alleviate the problem by leveraging existing datasets which provide image-level annotations only.

In the common Multiple Instance Learning (MIL) formalization of the WSD problem, an image I , associated with a label of a given class y , is described as a “bag” of Bounding Boxes (BBs), where at least one BB is a positive sample for y and the others are samples of the other classes (e.g., the background class). The main problem is how can the classifier, while being trained, automatically guess what the positives in I are. A typical MIL-based solution alternates between 2 phases: (1) optimizing the classifier’s parameters, assuming that the positive BBs in each image are known, and (2) using the current classifier to predict the most likely positives in each image [9], [28]. However, a well known problem of MIL-like solutions is that if the initial classifier is

not strong enough, this process can easily drift. For instance, predicted false positives (e.g., BBs on the background) can make the classifier learn something different than the target class.

Kumar et al. [22] propose to alleviate this problem using a *self-paced* learning strategy. The main idea is that a subset of “easy” samples can be automatically selected by the classifier in each iteration. Training is then performed using only this subset, which is less prone to drifting and is progressively increased in the subsequent iterations when the classifier becomes more mature. Self-paced learning, applied in many other studies [18], [23], [24], [26], [30], [39], [45], is related to *curriculum learning* [2] and is biologically inspired by the common human process of gradual learning, starting with the simplest concepts.

In this paper we adopt a self-paced learning approach to handle the uncertainty related to the BB-level localization of the objects in the training images in a WSD scenario, and “easier” is interpreted as “more reliable” localization. We propose a new training protocol for deep networks in which the self-paced strategy is implemented by modifying the mini-batch-based selection of the training samples. As far as we know, this is the first self-paced learning approach directly embedded in a modern end-to-end deep-network training protocol.

More specifically, the solution we propose in this paper is based on the state-of-the-art (fully supervised) object-detection architecture Fast-RCNN [12]. Fast-RCNN naturally embeds the idea of an image as a bag of BBs (see Sec. 3). Moreover, in the Fast-RCNN approach, each mini-batch of the Stochastic Gradient Descent (SGD) procedure is sampled hierarchically, by first (randomly) sampling images and then sampling BBs within those images according to the BB-level ground truth information. We exploit this

• Enver Sangineto, Moin Nabi and Nicu Sebe are with the Department of Information Engineering and Computer Science (DISI), University of Trento, Italy.

E-mail: enver.sangineto@unitn.it; sebe@disi.unitn.it

• Moin Nabi is also with SAP SE, Berlin, Germany.

E-mail: m.nabi@sap.com

• Dubravko Culibrk is with the Department of Industrial Engineering and Management, University of Novi Sad, Serbia.

E-mail: dculibrk@uns.ac.rs

[†] These two authors contributed equally.

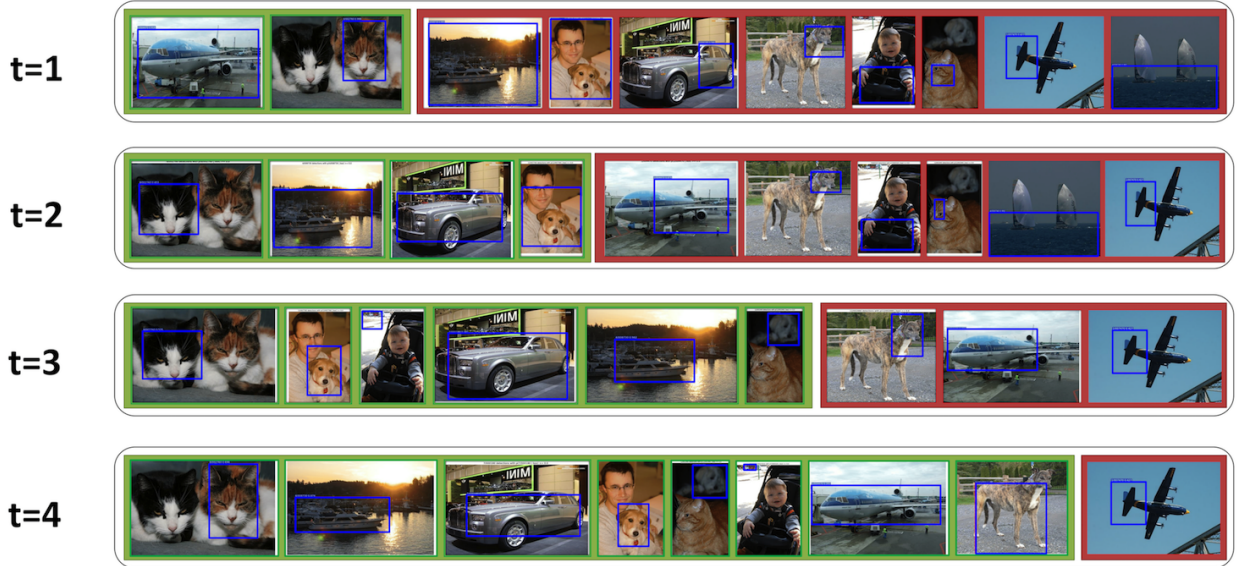


Fig. 1. A schematic illustration of how the training dataset T_t (represented by the green rectangle) of our deep network evolves depending on t and on the progressively increasing recognition skills of the trained network.

“image-centric” sampling but we modify the random image selection using a self-paced strategy in which the images containing the highest-confidence boxes associated with the annotated classes are selected the first. In more detail, given an image I with an image-level label y , we use the network trained in the previous iterations to associate a class-specific score s_{iy} with each *predicted BB* p_i . The highest-score box z^I over all these predictions is selected in I . Note that, due to the spatial regression layer in Fast-RCNN, all the predicted BBs (z^I included) are usually different from the set of input box proposals, i.e., the bag of BBs associated with I dynamically changes at every self-paced iteration. Once z^I is chosen for each I in the training set, we select a subset of images according to the score associated with the corresponding z^I and a mini-batch of positive and background BBs is extracted using z^I . Moreover, since we train a multi-class classifier (a common approach in deep networks which exploit inter-category representation sharing [21]), we exploit the competition among classifiers of different categories (i.e., among different classification-output neurons of the same network) and an image is chosen only when its label is consistent with the strongest classifier on that image. This image-based classifier competition is also used to progressively train different classifiers starting from the strongest ones. Since the predictions of the weak classifiers are usually not correct, we start training using only those samples corresponding to the strongest classifiers (i.e., the easiest classes), which are selected according to the number of images in which each classifier beats all the others. The benefit of this strategy is that, during the initial training phases, the network learns a visual representation of the objects in the shared layers (common to all the classes) together with a representation of the background class and these improved representations are used in the subsequent training phases when the network predicts the object localizations of the difficult classes.

Note that the basic Fast-RCNN architecture has been

used, simulated or extended in many different applications, due to the flexibility of its region-based pooling layer, including a few very recent WSD architectures [5], [19], [25]. Since we propose a *training protocol*, our method is orthogonal to many of these works and can potentially be used in conjunction with more sophisticated architectures to obtain higher accuracy experimental results. However, we adopted the basic Fast-RCNN architecture [12] in order to present a more general framework and we show empirical results using both a low-capacity AlexNet-like network [21] and a much larger VGG-16 network [36]. In common WSD benchmarks (Pascal VOC 2007 and 2010, and ILSVRC 2013) our approach largely outperforms the current state of the art. For instance, on ILSVRC 2013, our AlexNet-based results are even higher than those results obtained by other WSD methods which use much larger capacity networks (e.g., VGG-16).

Finally, as far as we know, this is the first work empirically showing that a self-paced selection of samples is useful in training a deep network. Recent works have shown that an *anti-curriculum learning* strategy (e.g., hard-negative mining) can be useful in a supervised scenario [33], [35]. In [34], [44] a *curriculum learning* strategy is used to select easy samples for training. However, the sample order is not decided by the classifier being trained (i.e., the network) but it is provided using auxiliary data (e.g., the program complexity in [44] and the object’s scale estimate in [34]). In our case, we do not use auxiliary data and we assume that only image-level labels are given at training time. The goal of the adopted self-paced strategy is to *discard noisy training data* (wrong pseudo-ground truth BBs) and we use the same detection network that is being trained in order to progressively select the most likely candidate pseudo-ground truth BBs.

In summary, our contributions are the following,

- We propose a computationally efficient self-paced learning protocol for training a deep network for

WSD. During the training of the network, the same network, at different evolution stages, is used to predict the object-level localizations of the positive samples and to select a subset of images whose pseudo-ground truth is the most reliable.

- We propose to use the spatial regression layer of the network to dynamically change the initial bag of boxes. We empirically show that selecting z^I over the set of current predictions ($\{p_i\}$) rather than over the set of the initial box proposals ($\{b_i\}$) can largely boost the final WSD accuracy.
- We propose to use class-specific confidence and inter-classifier competition to decrease the probability of selecting incorrect samples.
- We propose to extend the self-paced sample selection paradigm to a self-paced class selection using the inter-classifier competition to estimate the difficulty of each class.
- We test our approach on Pascal VOC 2007, Pascal VOC 2010 and ILSVRC 2013, obtaining state-of-the-art WSD results in all these benchmarks. This is the first work showing the usefulness of a self-paced sample selection strategy with an end-to-end trained deep network.

Our code and our trained models are publicly available¹. The rest of the paper is organized as follows. In Sec. 2 we review the literature concerning self-paced learning, weakly supervised object detection and related areas. In Sec. 3 we analyse the main aspects of the Fast-RCNN architecture that are of interest for our work. In Secs. 4-5 we introduce and analyse our method, which is evaluated in Secs. 6-7 and finally we conclude in Sec. 8.

2 RELATED WORK

Many recent studies have shown that selecting a subset of “good” samples for training a classifier can lead to better results than using all the samples [23], [24], [32], [39], [42]. A pioneering work in this direction is the *curriculum learning* approach proposed in [2]. The authors show that suitably sorting the training samples, from the easiest to the most difficult, and iteratively training a classifier starting with a subset of easy samples (progressively augmented with more and more difficult samples), can be useful to find better local minima. In [7], easy and difficult images (taken from datasets known to be more or less “difficult”) are provided for training a Convolutional Neural Network (CNN) in order to learn generic CNN features using weakly annotated data. In [43], different and progressively more complex CNNs are trained for a segmentation task, using more and more difficult data samples together with the output of the previously learned networks. It is worth noting that in these and in all the other curriculum-learning-based approaches, the order of the samples is decided using additional supervisory information usually provided by a human teacher. Unfortunately, these “image-easiness” meta-data are not available for the common large-scale datasets.

Curriculum learning was extended to *self-paced* learning in [22]. The main difference between the two paradigms

is that in self-paced learning the order of the samples is automatically computed and it is a priori unknown. The selection of the best “easy” sample set for training is, generally speaking, untractable (it is a subset selection problem). The solution proposed in [22] is based on a continuous relaxation of the problem’s constraints which leads to a biconvex optimization of a Structural SVM. Supancic et al. [39] adopt a similar framework in a tracking by detection scenario and train a detector using a subset of video frames, showing that this selection is important to avoid drifting. Frames are selected by computing the SVM objective function for different candidate subsets of frames and then selecting the subset corresponding to the lowest objective value. In [18] the authors pre-cluster the training data in order to balance the selection of the easiest samples with a sufficient inter-cluster diversity. However, the clusters and the feature space are fixed: they do not depend on the current self-paced training iteration and the adaptation of this method to a deep-learning scenario, where the feature space changes during learning, is not trivial. In [30] a set of learning tasks is automatically sorted in order to allow for a gradual sharing of information among tasks. Our self-paced *class* selection aims at a similar goal but it is obtained with a radically different approach. Liang et al. [26] use Exemplar SVMs (ESVMs) [27] to train a classifier from a single positive sample. The trained ESVMs are then run on an unsupervised collection of videos in order to extract new positives which are gradually more and more different from the seed instances. ESVMs are also used in [23] to assess the “training value” of each instance and then use this value to select the best subset of samples for training a classifier. In [24], the easiness of an image region is estimated using its “objectness” and the category context of its surrounding regions. In [45] saliency is used to progressively select samples in WSD.

Although some of these self-paced methods use pre-trained CNN-based features to represent samples (e.g., [18], [26]), none of them uses a deep network as the classifier or formulates the self-paced strategy in an end-to-end deep-network training protocol as we do in this paper.

Concerning the broader WSD field, a few recent studies address the problem in a deep-learning framework. For instance, in [29], a final max-pooling layer selects the highest scoring position for an instance of an object in the input image and back-propagates the training error only to those network’s weights that correspond to the highest scoring window. However, in this work the object is localized at testing time by providing only one 2D point. A similar max-pooling layer over different subwindows of the input image is adopted in [14], together with the Fast-RCNN architecture [12], to select the most significant context box in an action recognition task. Hoffman et al. [16] use both weakly-supervised and strongly-supervised data (the latter being BB-level annotations) to adapt a CNN pre-trained for a classification task to work in a detection task. This work was extended in [17] using a MIL-based SVM training. Encouraging results were obtained both in [16] and in [17] using the ILSVRC 2013 detection dataset. However, in both papers, auxiliary strongly-annotated data for half of the 200 ILSVRC 2013 categories were used for training, together with image-level-only annotations for the remaining categories.

1. <https://github.com/moinnabi/SelfPacedDeepLearning>

Very recently, a few WSD approaches have been proposed for training a deep network in an end-to-end fashion which are based on specific network architectures. For instance, Bilen and Vedaldi [5] extend a Fast-RCNN-like network using two different data streams, respectively computing a classification and a detection score for each candidate box of an image. Specifically, the detection score is obtained using a softmax operator which produces a probability distribution over all the input region proposals, thus avoiding the hard assignment of the pseudo-ground truth position to a specific box, common in MIL-like approaches. A similar soft assignment in a WSD scenario was previously developed in [3], [4], while the architecture proposed in [5] is further extended in [19] introducing specific regions which describe the context surrounding each candidate box. We compare with [3], [4], [5] and [19] in Sec. 6.

Li et al. [25] address the multi-label problem (the same image can contain objects belonging to different classes) by proposing a specific classification loss for training an image *classification* network. Then, this classification network is used to initialize a Fast-RCNN-based *detector* which is trained using a MIL framework. Following their approach we trained a similar classification network which is used as the initialization of our detector, trained using our self-paced framework and tested on Pascal VOC, where we largely outperform the results obtained in [25]. In [40] for each candidate box of an image, an *attention score* is computed which estimates how likely that box contains the object of interest. While these works propose specific network *architectures* for solving the WSD problem, we take a different direction and we propose a *training protocol* which can be used with different architectures, provided that they have a region-pooling layer similar to Fast-RCNN and an image-based sampling strategy in computing the SGD mini-batch (Sec. 3).

Finally, the closest work to this paper is probably [34], where the authors propose a curriculum-learning based training protocol for WSD, in which the size estimate of an object inside a given image is used as a proxy for assessing the “easiness” degree of that image. However, an additional training set, provided with the ground-truth size of each object, is necessary to train the size regressor, which makes this approach not directly comparable with other works using only weakly-supervised data. Moreover, the authors present results using either SVM classifiers or a deep network (Fast-RCNN). In the latter case, the deep network is trained using a simpler MIL approach in which the previous SVM-self paced based image selection is used only to select an initial set of pseudo-ground truth for training. Differently from [34], our pseudo-ground truth training set is modified during the Fast-RCNN training.

3 FAST-RCNN AND NOTATION

In this section we review the main aspects of the Fast-RCNN [12] approach which are important to understand our proposal and we introduce notations, used in the rest of the paper.

The *supervised* state-of-the-art object-detection approaches [12], [15], [35] on Pascal VOC [10], [11] are based on the Fast-RCNN architecture, whose main characteristic is

the *RoI pooling layer*. This layer is used to extract box-specific information from the final convolutional maps and feed the final classification and regression branches of the network.

The network takes as input an image I (raw pixels) and a set of BBs on I : $B(I) = \{b_1, \dots, b_n\}$. $B(I)$ is computed using an external tool, which usually selects image subwindows taking into account their “objectness”: for instance using Selective Search [41] (also used in all our experiments). If f is the function computed by the network, its outcome is a set of detections:

$$f(I, B(I)) = \{d_{ic}\}_{i=1, \dots, n, c=1, \dots, C}, \quad (1)$$

where C is the number of object classes and, for each class c and each input box $b_i \in B(I)$, $d_{ic} = (s_{ic}, p_{ic})$, where s_{ic} is the score and p_{ic} the predicted box. Note that, usually, $p_{ic} \neq b_i$ and $p_{ic} \notin B(I)$, p_{ic} being the result of a spatial regression applied to b_i . The RoI pooling layer makes it possible to efficiently compute $f(I, B(I))$ and the dependence of the network’s output on a set of boxes $B(I)$ is important for our bag of BBs formulation.

As mentioned in Sec. 1, another aspect of Fast-RCNN exploited in our training protocol is that each mini-batch (used in the mini-batch SGD procedure) is constructed using only a small number m of images, where $m = 2$ is indicated as a good compromise between quality of the samples and efficiency. Specifically, at training time a set $T = \{(I_1, G_1), \dots, (I_j, G_j), \dots, (I_N, G_N)\}$ of N images and corresponding ground-truth is given, where: $G_j = \{(y_1, b_1), (y_2, b_2), \dots\}$ and, for each (y_i, b_i) , $y_i \in \{1, \dots, C\}$ is the label and $b_i \in B(I)$ is the BB of the i -th object instance in I . In each SGD iteration $m = 2$ images are randomly extracted from T . If I_j is one of these 2 images, for each $(y_i, b_i) \in G_j$, b_i is matched with the boxes in $B(I)$ using common spatial criteria (i.e., Intersection over Union between two BBs higher than a given threshold) in order to select those BBs in $B(I)$ that will be used as positives for the y_i class, as well as a set of “negatives” (i.e., samples for the background class $y = 0$).

For more details we refer the reader to [12]. What is important to highlight here is that Fast-RCNN is a strongly supervised method. Conversely, in our weakly-supervised scenario, we do not have BB-level annotations. Hence, in the rest of the article we assume that our training set is $T = \{(I_1, Y_1), \dots, (I_j, Y_j), \dots, (I_N, Y_N)\}$, where $Y_j = \{y_1, \dots, y_{n_j}\}$ is the set of labels associated with image I_j and the number of object classes contained in I_j varies depending on the specific image ($n_j \geq 1$). Note that, for a given class $y_i \in Y_j$, more than one object of the same class can be contained in I_j : for instance, two instances of the “dog” category; and the number of instances is unknown.

Since object-level ground truth is not given, we use the network (in the current self-paced training iteration) to compute the most likely positions of the objects in I_j . In the next section we show how these locations are computed and how T is updated following a self-paced learning strategy.

4 SELF-PACED LEARNING PROTOCOL

We call W the set of weights of all the layers of the network and we initialize our network with W_0 , which can

Algorithm 1 Self-Paced Weakly Supervised Training

Input: T, W_0, r_1, M

Output: Trained network f_{W_M}

- 1 For $t := 1$ to M :
- 2 $P := \emptyset, T_t := \emptyset$
- 3 For each $(I, Y) \in T$:
 - 4 Compute (s_y^I, z_y^I) using Eq. 2
 - 5 If $y \in Y$, then: $P := P \cup \{(I, s_y^I, z_y^I, y)\}$
- 6 For each $c \in \{1, \dots, C\}$ compute $e(c)$ using Eq. 3
- 7 $C_t := r_t C$
- 8 Let $S = \{c_1, c_2, \dots\}$ be the subset of the C_t easiest classes according to $e(c)$
- 9 Remove from P those tuples (I, s, z, y) s.t. $y \notin S$
- 10 $N_t := \min(r_t N, |P|)$
- 11 Let P' be the N_t topmost tuples in P according to the s -score
- 12 For each $(I, s, z, y) \in P'$: $T_t := T_t \cup \{(I, \{(y, z)\})\}$
- 13 $V_0 = W_{t-1}$
- 14 For $t' := 1$ to N_t/m :
 - 15 Randomly select $(I_1, \{(y_1, z_1)\}), \dots, (I_m, \{(y_m, z_m)\}) \in T_t$
 - 16 Compute a mini-batch MB of BBs using $(I_1, \{(y_1, z_1)\}), \dots, (I_m, \{(y_m, z_m)\})$
 - 17 Compute $V_{t'}$ using MB and back-propagation on $f_{V_{t'-1}}$
- 18 $W_t := V_{N_t/m}$
- 19 $r_{t+1} = r_t + \frac{1-r_1}{M}$

be obtained using any standard object *classification* network, *trained using only image-level information*. At the end of this section we provide more details on how W_0 is obtained.

The proposed self-paced learning protocol of the network is composed of a sequence of *self-paced iterations*. At a self-paced iteration t we use the current network $f_{W_{t-1}}$ in order to select a subset of easy classes and easy samples of these classes. The result is a new training set T_t which is used to train a new model W_t . W_t is obtained using the “standard” training procedure of the Fast-RCNN (Sec. 3), based on mini-batch SGD, but it is applied to T_t only and iterated for only N_t/m mini-batch SGD iterations, N_t being the cardinality of T_t . Note that, being m the number of images used to build a mini-batch, N_t/m corresponds to one epoch (a full iteration over T_t). Note also that a mini-batch SGD iteration is different from a self-paced iteration and in each SGD iteration a mini-batch of BBs is formed using the pseudo-ground truth obtained using $f_{W_{t-1}}$. The proposed protocol is summarized in Alg. 1 and we provide the details below.

Computing the latent boxes. Given an image I , its label set Y and the current network $f_{W_{t-1}}$, first we compute:

$$(s_y^I, z_y^I) = \arg \max_{(s_{ic}, p_{ic}) \in f_{W_{t-1}}(I, B(I))} s_{ic} \quad (2)$$

In Eq. 2, (s_y^I, z_y^I) is the detection in $f(I, B(I))$ with the highest score (s_y^I) with respect to all the detections obtained starting from $B(I)$ and the subscript y indicates the corresponding class. z_y^I is a *latent box* which specifies the most

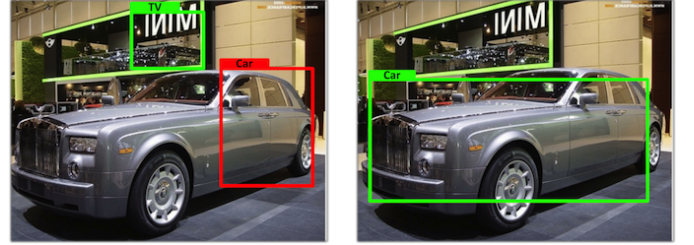


Fig. 2. Inter-classifier competition. The two above figures show the behaviour of our self-paced learning algorithm on the same image I in two different iterations ($t = 1$ and $t = 2$). In both cases, the green box shows the highest-score box in I corresponding to z_y^I in Eq. 2. Conversely, the red box in the left figure shows the highest-score box in I corresponding to the *car* class (z_{car}). Since in $t = 1$ (left figure) $s_{TV} = s_y^I > s_{car}$, and since $TV \notin Y$, then I is not included in T_1 (see also Fig. 1). However, in $t = 2$ (right figure) $s_{TV} < s_y^I = s_{car}$ (where $car \in Y$), thus $(I, s_{car}, z_{car}, car)$ is included in P (line Line 5 in Alg. 1): the “car” classifier in this iteration is strong enough and “wins” in I .

likely position of an object of the “winning” class y in image I according to $f_{W_{t-1}}$. Note that the background class is not included in $f_{W_{t-1}}$ (see Eq. 1), thus $y \in \{1, \dots, C\}$. Note also that z_y^I is computed using the regression layer of $f_{W_{t-1}}$ and usually $z_y^I \notin B(I)$. Conversely, most of the existing WSD approaches [5], [19], [25], [34], [40] restrict the choice of the pseudo-ground truth over a pre-fixed and constant set of region proposals ($B(I)$). We empirically show in Sec. 7.1 the importance of using the regression part of the network to extend $B(I)$. However, at the end of the current iteration t , z_y^I and all the other predictions $\{p_{ic}\}$ are discarded and, at iteration $t + 1$, Eq. 2 is minimized again starting from the original set of box proposals $B(I)$.

If $y \in Y$ (y is one of the labels of I), then we associate I with the latent box z_y^I and with the confidence score s_y^I (line 5), otherwise I is temporally discarded and will not be included in the current self-paced iteration training set T_t .

Inter-classifier competition. Eq. 2 imposes a competition among classifiers, where a “classifier” for class c is the classification-output neuron of f specific for class c . Only if one of the classifiers *corresponding to an image label* $y \in Y$ is “stronger” (more confident) than all the others, including $y' \notin Y, y' \neq 0$, then I is considered for inclusion in T_t (Line 5). We found this competition to be very important to decrease the risk of error and to enforce a self-paced learning strategy which prudently selects initially easy image samples. When the network becomes more mature (i.e., in the subsequent self-paced iterations), the risk of error gradually decreases and a previously weaker classifier can correctly “win” a previously discarded image (see Fig. 2).

Note that a consequence of this classifier competition is that only one pseudo-ground truth box z_y^I can be selected from a given image I , regardless of the number of labels associated with I and the number of object instances of class y in I . In Sec. 7.2 we present multiple-label and multiple-instance relaxations of this inter-classifier competition.

Class selection. The classifier competition is used also to sort all the C classes from the easiest to the most difficult. This is obtained using the winning classifiers in each image

as follows. Let $P = \{(I_1, s_1, z_1, y_1), (I_2, s_2, z_2, y_2), \dots\}$ be the set of non-discarded images at iteration t (Line 5) and let:

$$e(c) = |\{(I, s, z, y) : (I, s, z, y) \in P, y = c\}|/p_c \quad (3)$$

be the “easiness” degree of class c , defined as the ratio between the cardinality of those tuples in P associated with the class label $y = c$ over the overall frequency of the label c in T (p_c). The higher the value $e(c)$ for a given class c , the stronger the corresponding classifier is and the easier that class according to $f_{W_{t-1}}$. We sort all the classes using $e(c)$ ($c = 1, \dots, C$) and we select the subset of the easiest $r_t C$ classes which are the only classes subject to training in the current self-paced iteration. The ratio $r_t \in [0, 1]$ is increased at each self-paced iteration (see below) and at iteration $t + 1$ more difficult classes will be included in T_{t+1} and presented to the network for training.

Selecting the easiest image samples. Once image samples associated with difficult classes have been removed from P (Line 9), we select a subset (T_t) of P corresponding to those images in which $f_{W_{t-1}}$ is the most confident. With this aim we use the score s_y^I computed using Eq. 2 and we sort P in a descending order according to these scores. Then we select the first N_t top-most elements, where $N_t = \min(r_t N, |P|)$, and $r_t N$ is an upper bound on the number of elements of T to be selected in the current self-paced iteration. At each self-paced iteration r_t is increased. Indeed, we adopt the strategy proposed in [22] (also used in most of the self-paced learning approaches) to progressively increase the training set as the model is more and more mature (see Fig. 1). However, in our experiments we observed that usually $|P| < r_t N$, mainly because of the sample rejection step in Line 5, hence the learning “pace” is dominated by our classifier-competition constraint.

Details. The inner loop over t' (Lines 14-17), whose number of iterations depends on the length of the current training set T_t , is equivalent to the mini-batch SGD procedure adopted in [12], with a single important difference: Since we do not have BB-level ground truth, each mini-batch is computed using (y, z) as the pseudo-ground truth (Line 12). MB is built using BB samples which are collected using the same spatial criteria adopted in the supervised Fast-RCNN training protocol (see Sec. 3) and with the same positive/negative proportion (see [12] for more details). Also the number of images $m = 2$ we use to compute a mini-batch of BBs is the same used in [12]. In this loop, the weights of the network are called $V_{t'}$ for notational convenience (their update depends on t' and not on t), but there is only one network model, continuously evolving.

Inspired by [22], where half of the data are used in the first self-paced iteration and all data are used in the last iteration, we start with $r_1 = 0.5$ and we iterate for $M = 4$ iterations till $r_M = 1$, linearly interpolating the intermediate increments (Line 19). Experiments with $M = 5$ obtained very similar results. All the other Fast-RCNN specific hyperparameters are the same used in [12] for the fine-tuning of a pre-trained network, including the initial learning rate value (0.001), the size of MB (128), the weight decay (0.0005) and the momentum (0.9). No batch normalization is used

and standard backpropagation with momentum is adopted. The only difference with respect to [12] is that, in all our experiments, we divide (only once) the learning rate by a factor of 10 after the first self-paced iteration.

The reason for which we adopted the same hyper-parameter values used in the supervised Fast-RCNN and we followed as strictly as possible the same design choices (e.g., how a mini-batch is computed, etc.) is that tuning the hyper-parameter values in a weakly supervised scenario is not easy because of the lack of validation data with BB-level ground truth. Moreover, in this way our training protocol can be more easily generalized to those WSD approaches which are based on the same Fast-RCNN architecture. All the above hyper-parameters (including those which are specific of our self-paced protocol, r_1 and M) are kept fixed in our experiments on both Pascal VOC and ILSVRC.

Finally, in all our experiments, T is composed of the original images and their mirrored versions. No other data augmentation is performed.

Computational issues. From a computational point of view, the only additional demanding operation in our approach with respect to the Fast-RCNN training procedure is computing $f(I, B(I))$ for each $I \in T$, which involves passing I forward through all the layers of f . Fortunately, Fast-RCNN performs this operation in only ≈ 0.1 seconds per image (e.g., using a Tesla K40 GPU). For instance, with $N = 20K$, computing the latent boxes of all the images in T takes approximately 30 minutes. Note that this operation is repeated only M times during the whole training.

A simpler self-paced approach to train a Fast-RCNN is to *fully* train the network (for several epochs) with an initial, small “easy” dataset T_1 , then use the current network to compute the latent variables of a larger set T_2 , then *fully* fine-tune the network again, etc. However, this procedure is not only much slower than the epoch-based dataset update strategy we adopted (because it involves a full-training of the detector for each iteration), but it is also less effective. Our preliminary results using this approach showed that the network quickly overfits on the initial relatively small dataset T_1 and the final accuracy of the network is much lower than what we obtain using Alg. 1.

Initialization. The initial model W_0 can be obtained in different ways using only weakly-supervised annotation. Below we describe the steps we followed in our experiments on Pascal VOC and on ILSVRC as solution examples.

In both datasets we used a two-steps procedure: (1) training a Classification Network (CN) and (2) inspired by [22], where *all* the samples of the dataset are used for pre-training the classifier using a small number of iterations, we also pre-train the Detection Network (Fast-RCNN) using all the images of T for a fixed, small number of SGD iterations.

In case of the ILSVRC dataset, the CN is obtained following the steps suggested in [16], [17]: Starting from the AlexNet [21], pre-trained on ImageNet (1000 classes), we first fine-tune the network on the ILSVRC 2013 detection dataset [31], which is composed of $C = 200$ classes. This is done by removing the last layer from the AlexNet and replacing it with a 200-class output layer. For the fine-tuning we use a random subset of the *train* partition of ILSVRC

2013 (see Sec. 6), but we simulate a situation in which we have access to *image-level labels only*. We call h^I this CN and W_{CN}^I its weights, where the superscript I stands for “trained on ILSVRC 2013”. Note that h^I takes as input a 227×227 image and outputs a 200-element score vector.

Using W_{CN}^I we initialize the Fast-RCNN architecture. To do so, the last layer needs again be removed and replaced by two (parallel) Fast-RCNN specific layers: a $C + 1$ classification layer and $C \times 4$ regression layer [12]. The weights of this layers are randomly initialized. Then, we train the Fast-RCNN Detection Network (DN) for $30K$ SGD iterations using all the images in T , where T is the *val1* split of ILSVRC 2013 (see Sec. 6), mirrored images included. Since Fast-RCNN is a DN and needs BB-level annotation for training, we associate the images in T with a pseudo-ground truth by collecting the top-score boxes obtained using h^I . More in detail, for each $(I, Y) \in T$ and each box $b \in B(I)$, we rescale b to 227×227 ($u(b)$) and, for each $y \in Y = \{y_1, \dots, y_k\}$, we compute:

$$z_y = \arg \max_{b \in B(I)} h^I(u(b), y), \quad (4)$$

where $h^I(\cdot, y)$ is the y -class score. The final pseudo ground-truth corresponding to I is $G = \{(y_1, z_{y_1}), \dots, (y_k, z_{y_k})\}$ (see Sec. 3). We call this training protocol *Init* and you can think of it as a one-shot MIL solution with only one iteration over the latent variables (i.e., the latent boxes are not recomputed while the network is trained and are kept fixed). Note that there is no classifier competition or class selection in *Init* and we use all the samples in T , inspired by Kumar et al. [22], confirming that this strategy leads to a good initialization for a self-paced learning approach. At the end of *Init*, we call the final network’s weights W_0^I and we use W_0^I as input in Alg. 1.

In case of Pascal VOC we use a similar strategy and we train different CNs for different experiments, using as basic architecture either AlexNet or VGG-16 [36]. Firstly, we simply use the above-mentioned h^I trained on ILSVRC 2013: the weights (W_{CN}^I) of h^I are directly used to initialize the Fast-RCNN architecture (except the last randomly initialized layers, see above). Moreover, the pseudo-ground truth for the *Init* stage is collected using Eq. 4 with an amputated version of h^I , obtained by removing 180 over 200 output neurons and keeping only those *fc8* original neurons roughly corresponding to the 20 Pascal VOC classes². We run *Init* for $10K$ SGD iterations using the *trainval* split of Pascal VOC 2007 (see Sec. 6) as our T . We call $W_0^{I,P}$ the final network’s weights because they are obtained using a hybrid solution, based on training images from both ILSVRC 2013 and Pascal VOC 2007. Note that, due to the differences between ILSVRC and Pascal VOC in both the corresponding *image distributions* and the *object classes* [1], [13], [20], using h^I to initialize *Init* corresponds to a quite weak initialization. Despite this, our experimental results show

2. Specifically, the adopted ILSVRC → VOC class mapping is: *airplane* → *aeroplane*, *bicycle* → *bicycle*, *bird* → *bird*, *watercraft* → *boat*, *wine bottle* → *bottle*, *bus* → *bus*, *car* → *car*, *domestic cat* → *cat*, *chair* → *chair*, *cattle* → *cow*, *table* → *diningtable*, *dog* → *dog*, *horse* → *horse*, *motorcycle* → *motorbike*, *person* → *person*, *flower pot* → *pottedplant*, *sheep* → *sheep*, *sofa* → *sofa*, *train* → *train*, *tv* or *monitor* → *tvmonitor*.

a surprisingly good accuracy achieved after the proposed self-paced training procedure (see Sec. 6).

In case of Pascal VOC, we also fine-tune a second CN, using only Pascal VOC 2007 *trainval*. Also in this case the basic network architecture is AlexNet, pre-trained on ImageNet (1000 classes). However, since Pascal VOC 2007 *trainval* is a much smaller dataset than the ILSVRC 2013 *train* split and, on average, a Pascal VOC image contains more objects with different-labels than an ILSVRC 2013 image [13], care should be taken in training a CN directly on Pascal VOC. For this reason we adopted the approach proposed in [25] for training a CN on a multi-label dataset, where the authors replace the network *softmax* loss with a multi-label loss based on a $2C$ binary element vector label. The trained CN (h^P) and the corresponding weights (W_{CN}^P) are used to collect pseudo-ground truth data and to initialize the Fast-RCNN for the *Init* stage (see above), using the same number ($10K$) of SGD iterations and the final weights are called W_0^P . Finally, in Sec. 6 we also show two experiments (Tab. 5 and Tab. 7) in which the basic architecture is VGG-16 and the initialization procedure is the same followed in case of W_0^P . To simplify our notation, we call the VGG-16 based initialization \tilde{W}_0^P as well and we will explicitly specify when the basic architecture is not AlexNet.

5 DISCUSSION

As mentioned in Sec. 1, the goal of the proposed self-paced strategy is to discard noisy data in order to decrease the drifting problem in a MIL framework. Hence, the training protocol described in Alg. 1 can be seen as a “prudent” strategy, where “good” (“easy”) data are preferred to lot of data. Moreover, Alg. 1 can terminate without using all T . In fact, in our experiments this often happens, and it is mainly due to the inter-classifier competition constraint. This is apparently in contrast with the common deep-learning training practice, where the trend is to use as much data as possible. However, in a WSD scenario, adding data which are wrong (noisy) most likely does not improve the training quality. For instance, Fig. 3, first column, shows the *class-specific* top score box z_y for a set of random image samples, computed taking into account the corresponding image label (y) and without inter-classifier competition. In a typical MIL-like approach z_y is selected as pseudo-ground truth, and in most of the cases these data are very noisy. Conversely, our self-paced learning strategy leads to select (and use) z_y only in later stages, most of the times decreasing the overall amount of noise (see Fig. 3, columns 1-4).

It is also worth noticing that our choice of using T_t for only one epoch of SGD-training is important to avoid overfitting, especially when $N_t = |T_t|$ is initially small (see the *Computational issues* paragraph).

Finally, the sequence of datasets T_1, \dots, T_M is not monotonic, meaning that an image $I \in T_{t_1}$ can be discarded when T_{t_2} is created (with $t_1 < t_2$). Empirically we observed frequent oscillations in the class-specific Average Precision (AP) when training both on Pascal VOC 07 and on ILSVRC 2013. However, the overall mean AP is almost monotonic with respect to the self-paced iterations, with some small oscillations (typically less than 1%), showing that the combined effect of weight sharing among classes and the com-

mon background class (whose samples are included in each mini-batch, independently of the positive class y) leads the network as a whole to benefit from the progressive increase of training data through time. In Sec. 7.1 we analyse this progressive behaviour of our networks and we contrast it with respect to other MIL-like solutions.

6 DETECTION PERFORMANCE

In this section we compare our method with other WSD approaches using the two most common WSD datasets (Pascal VOC and ILSVRC 2013). Comparing to each other different methods developed in the past years is not easy due to their heterogeneity, which has been increased after the introduction of deep-learning approaches. For instance, some methods [8] use SVMs and hand-crafted features, others [3], [4], [9], [37], [38], [42] use SVMs and pre-trained CNN-features obtained with the AlexNet and very recently a few deep learning approaches based on an end-to-end training [5], [19], [25], [34], [40] have been introduced (including ours). Moreover, the latter usually present results obtained with small (e.g. AlexNet [21]), medium (e.g. VGG-CNN-M-1024 from [6]) or large (e.g. VGG-16 [36]) capacity networks or using an ensemble of three or more architectures.

In order to have a comparison which is the most fair as possible, we separate methods based on low-capacity, AlexNet-like networks from those based on higher-capacity, VGG-16-like architectures and we mark those approaches which use ensembles of networks. In the rest of the paper, if not otherwise explicitly specified, the basic architecture used for our experiments (initialization included) is AlexNet.

The ILSVRC 2013 detection dataset [31] is a standard benchmark for object detection. It is partitioned in 3 main subsets: *train*, *val* and *test*. The *train* images are more object-centric (one or very few objects per image on average) and represent more classification-style data than the images in the other 2 partitions [13], [16], [17]. All the images of the ILSVRC 2013 detection dataset are annotated with object-level ground truth that we do *not* use. We use *only* the labels of the objects contained in each image (where each label ranges over $C = 200$ classes). Girshick et al. [13] split *val* further in *val1* and *val2* and use at most 1000 randomly selected images per category from *train*. We use the same approach and $\approx 200K$ randomly selected images from *train* were used to fine-tune AlexNet and obtain h^I as explained in Sec. 4 and following the procedure suggested in [16], [17]. Then, we use *only* *val1* as our set T ($N \approx 20K$, after image mirroring). T is the training dataset used both in *Init* and in Alg. 1. Finally, we evaluate on *val2*, whose cardinality is $\approx 10K$ (the test images are not mirrored). Note that this is a broadly adopted protocol, both for supervised (e.g., [12], [13]) and weakly or semi-supervised (e.g., [16], [17], [25]) object detection experiments.

Once our network is trained using *Init* and Alg. 1, it is used as a standard detector at testing time. In other words, given a test image I , we apply Non-Maxima Suppression on $f(I, B(I))$ as in the original Fast-RCNN approach [12] and in this way we obtain *multiple, spatially separated detections* per category on I and we can compute Average Precision (AP) and mean Average Precision (mAP) following the standard object detection protocol [10].

In Tab. 1 we compare our approach with the previously published WSD results on ILSVRC 2013: Wang et al. [42] and Li et al. [25]. Our method largely outperforms the state of the art in this large dataset. Note that Li et al. [25] report other results obtained using a VGG network [36]: 10.8 mAP, which is lower than what we obtained with our self-paced training protocol using a much smaller network.

Method	End-to-end training	mAP
Wang et al. ^(*) [42]		6
Li et al. [25]	✓	7.7
Ours	✓	12.13

TABLE 1: Quantitative comparison (mAP %) on the ILSVRC 2013 detection dataset. All the methods are based on a single, low-capacity network (AlexNet). Wang et al. [42] use AlexNet to extract CNN-features from the BBs but do not perform end-to-end training. (*) Note that the result of Wang et al. [42] is obtained on the whole ILSVRC 2013 *val* set, while our result and the result of Li et al. [25] are computed on the *val2* split.

Pascal VOC 2007 [10] is another well known benchmark for object detection and it is widely used by different WSD methods [3], [4], [5], [8], [9], [19], [25], [34], [37], [38], [40], [42]. The number of classes (C) is 20. We adopted the common training-testing protocol in which training is done on the *trainval* split and testing is performed on the *test* split. Hence, T is *trainval* in which *only image-level labels were used*. Since *trainval* is highly imbalanced toward the *person* class, we have subsampled this class, selecting the 262 top-score images used in case of *Init*. Since we used different CNs to initialize the weights of our network (see Sec. 4), we report results obtained using $W_0 = W_0^{I,P}$ and $W_0 = W_0^P$ in Alg. 1, respectively. The results are shown in Tab. 2, where all the methods (including ours) use AlexNet (or an AlexNet-like) as the basic architecture. Using a CN trained on ILSVRC (h^I , see Sec. 4), the final mAP reached after the self-paced training (Alg. 1) is 32.1, which is comparable with other state-of-the-art WSD methods. Using a stronger initialization, in which the CN is trained using a multi-label loss [25] directly on Pascal VOC (h^P , Sec. 4), the final mAP after the self-paced training is 38.11, which is higher than all the other weakly supervised approaches tested on this dataset.

In order to show how large is the gain that can be obtained using the proposed self-paced training protocol, we compare the detection performance achieved when using only *Init* for fine-tuning the Fast-RCNN (see Sec. 4) with the performance obtained after the self-paced phase (*SP*) described in Alg. 1. Since *Init* is used to initialize Alg. 1, the accuracy difference shows the boost obtained by the self-paced strategy. The results, reported in Tab. 4, show that, independently of the CN used to initialize *Init*, in both cases the *SP*-based boost over the *Init* phase is dramatic: +7.36 mAP in case of h^I and +6.18 in case of h^P . Moreover, since we trained h^P as proposed by Li et al. [25], it is also interesting to directly compare the results we obtained using h^P and the results obtained in [25], where a *detection* network is trained on top of the same CN. Our “simple” *Init*-based detector achieves a slightly better mAP (31.93) than the mAP (31) achieved by the DN proposed in [25].

Method	End-to-end	aero	bike	bird	boat	bottle	bus	car	cat	chair	cow	table	dog	horse	mbike	persn	plant	sheep	sofa	train	tv	mAP
Song et al. [37]		27.6	41.9	19.7	9.1	10.4	35.8	39.1	33.6	0.6	20.9	10	27.7	29.4	39.2	9.1	19.3	20.5	17.1	35.6	7.1	22.7
Song et al. [38]		36.3	47.6	23.3	12.3	11.1	36	46.6	25.4	0.7	23.5	12.5	23.5	27.9	40.9	14.8	19.2	24.2	17.1	37.7	11.6	24.6
Bilen et al. [3]		42.2	43.9	23.1	9.2	12.5	44.9	45.1	24.9	8.3	24	13.9	18.6	31.6	43.6	7.6	20.9	26.6	20.6	35.9	29.6	26.4
Bilen et al. [4]		46.2	46.9	24.1	16.4	12.2	42.2	47.1	35.2	7.8	28.3	12.7	21.5	30.1	42.4	7.8	20	26.8	20.8	35.8	29.6	27.7
Cinbis et al. [9]		39.3	43	28.8	20.4	8	45.5	47.9	22.1	8.4	33.5	23.6	29.2	38.5	47.9	20.3	20	35.8	30.8	41	20.1	30.2
Wang et al. (*) [42]		48.9	42.3	26.1	11.3	11.9	41.3	40.9	34.7	10.8	34.7	18.8	34.4	35.4	52.7	19.1	17.4	35.9	33.3	34.8	46.5	31.6
Li et al. [25]	✓	49.7	33.6	30.8	19.9	13	40.5	54.3	37.4	14.8	39.8	9.4	28.8	38.1	49.8	14.5	24	27.1	12.1	42.3	39.7	31.0
Bilen et al. [5]	✓	42.9	56	32	17.6	10.2	61.8	50.2	29	3.8	36.2	18.5	31.1	45.8	54.5	10.2	15.4	36.3	45.2	50.1	43.8	34.5
Shi et al. (**) [34]	✓	-	-	-	-	-	-	-	-	-	-	-	-	-	-	-	-	-	-	-	36.0	
Kantorov et al. [19]	✓	57.1	52	31.5	7.6	11.5	55	53.1	34.1	1.7	33.1	49.2	42	47.3	56.6	15.3	12.8	24.8	48.9	44.4	47.8	36.3
Ours ($W_0^{I,P}$)	✓	49.2	43.7	34.9	26.11	3.9	47.8	53.3	48.4	13.8	14.7	0.7	28.1	36.6	49.3	21.7	16.7	26.8	31.9	52.5	42	32.1
Ours (W_0^P)	✓	50.1	52.4	35.8	22.9	13.4	55.3	56.3	58.9	17.7	46.2	30.1	40.3	44.6	57.5	8.6	16.2	39.7	24.5	54.6	37.1	38.11

TABLE 2: Quantitative comparison (AP %) on the Pascal VOC 2007 *test* set. All the methods are based on a single network with a capacity comparable with AlexNet, which is used either as a black-box to extract CNN-features or to perform end-to-end training (see the corresponding column). Note that: (*) Wang et al. [42] specifically tune the number of latent categories for each class and (**) Shi et al. [34] use additional data (the Pascal VOC 2012 dataset) with BB-level annotation at training time.

Method	End-to-end	aero	bike	bird	boat	bottle	bus	car	cat	chair	cow	table	dog	horse	mbike	persn	plant	sheep	sofa	train	tv	avg
Bilen et al. [4]		66.4	59.3	42.7	20.4	21.3	63.4	74.3	59.6	21.1	58.2	14	38.5	49.5	60	19.8	39.2	41.7	30.1	50.2	44.1	43.7
Cinbis et al. [9]		65.3	55	52.4	48.3	18.2	66.4	77.8	35.6	26.5	67	46.9	48.4	70.5	69.1	35.2	35.2	69.6	43.4	46.6	43.7	52.0
Wang et al. (*) [42]		80.1	63.9	51.5	14.9	21	55.7	74.2	43.5	26.2	53.4	16.3	56.7	58.3	69.5	14.1	38.3	58.8	47.2	49.1	60.9	48.5
Li et al. [25]	✓	77.3	62.6	53.3	41.4	28.7	58.6	76.2	61.1	24.5	59.6	18	49.9	56.8	71.4	20.9	44.5	59.4	22.3	60.9	48.8	49.8
Bilen et al. [5]	✓	68.5	67.5	56.7	34.3	32.8	69.9	75	45.7	17.1	68.1	30.5	40.6	67.2	82.9	28.8	43.7	71.9	62	62.8	58.2	54.2
Shi et al. (**) [34]	✓	-	-	-	-	-	-	-	-	-	-	-	-	-	-	-	-	-	-	-	60.9	
Kantorov et al. [19]	✓	83.3	68.6	54.7	23.4	18.3	73.6	74.1	54.1	8.6	65.1	47.1	59.5	67	83.5	35.3	39.9	67	49.7	63.5	65.2	55.1
Ours ($W_0^{I,P}$)	✓	68.6	55.2	49	47	18	68.3	73.5	70.6	22.1	23.3	1.9	40.3	61	69.4	31.7	37.7	38.9	44.3	59.4	60.5	47.0
Ours (W_0^P)	✓	76.4	70.3	54.8	40.7	36.2	72	73.4	76.8	46	58.9	43.9	61.3	67.4	75	27	38.4	60.4	55.9	62.8	61.9	58.0

TABLE 3: Quantitative comparison (CorLoc %) on the Pascal VOC 2007 *trainval* set (with a single AlexNet-like capacity network). Note that: (*) Wang et al. [42] tune the number of latent categories for each class and (**) Shi et al. [34] use additional data with BB-level annotation at training time.

However, our full-pipeline *Init*+*SP* obtains a much higher mAP value (38.11), showing the advantage of a self-paced training strategy. The gap with respect to [25] is even higher in other experiments (e.g., see Tabs. 6-7). In Sec. 7.1 (Tab. 9) we show the corresponding relative boost obtained by *SP* with respect to *Init* in case of the ILSVRC dataset.

Classification Network		
	h^I	h^P
<i>Init</i>	24.74	31.93
<i>Init</i> + <i>SP</i>	32.1	38.11

TABLE 4: mAP (%) on Pascal VOC 2007 *test* computed using only *Init* (first row) or *Init*+*SP* (second row) for fine-tuning the detector. The first column corresponds to the results obtained when *Init* is initialized with a CN trained with only ILSVRC data (h^I), while the second column corresponds to using a CN trained with Pascal VOC data and a multi-label loss [25] (h^P).

In Tab. 3 we report the CorLoc computed on the *trainval* split, which is a common metric adopted in many WSD approaches tested on Pascal VOC 07. Our CorLoc result corresponding to the W_0^P -based initialization is the second best after the values obtained by Shi et al. [34].

Finally, in Tab. 5 we report the results obtained using a larger capacity network. Specifically, we use VGG-16 [36] and we compare with those works which use the same (single) network. In our case, VGG-16 is used both at initialization time, where we train a CN (h^P) following the steps

reported in Sec. 4, and for the Fast-RCNN DN, trained using our self-paced protocol (*Init*+*SP*). As shown in Tab. 5, we obtain state-of-the-art results, largely outperforming the other methods. The importance of this experiments relies on the fact that it demonstrates that our self-paced protocol is not inclined to overfitting with a large-capacity network.

Pascal VOC 2010 [11]. In Tabs. 6-7 we show the results obtained with the Pascal VOC 2010 *test* set. Tab. 6 refers to methods using an AlexNet-like network, while Tab. 7 refers to methods using a VGG-16 or an ensemble of VGG-16 and other networks. In both cases, our results are the state of the art. Specifically, our VGG-16 based results are even higher than previous results obtained with an ensemble of 3 networks [5].

7 ANALYSIS OF DIFFERENT ASPECTS OF THE PROTOCOL

In this section we analyse the influence of different elements of our proposed training protocol by separately removing or modifying important parts of Alg. 1.

7.1 Simplified versions of the training protocol

Basic-MIL. In the experiments of this subsection we use both Pascal VOC 07 and ILSVRC 2013. We start with comparing our method (Self-Paced, *SP*) with a MIL-based solution (*MIL*), where: (a) all the images in T are used and (b) in each image the latent boxes are computed by iteratively maximizing the *class-specific* score of the current

Method	aero	bike	bird	boat	bottle	bus	car	cat	chair	cow	table	dog	horse	mbike	persn	plant	sheep	sofa	train	tv	mAP
Li et al. [25]	54.5	47.4	41.3	20.8	17.7	51.9	63.5	46.1	21.8	57.1	22.1	34.4	50.5	61.8	16.2	29.9	40.7	15.9	55.3	40.2	39.5
Bilen et al. [5]	39.4	50.1	31.5	16.3	12.6	64.5	42.8	42.6	10.1	35.7	24.9	38.2	34.4	55.6	9.4	14.7	30.2	40.7	54.7	46.9	34.8
Shi et al. (*) [34]	-	-	-	-	-	-	-	-	-	-	-	-	-	-	-	-	-	-	-	-	37.2
Ours (W_0^P)	61.7	66.7	47.7	26.2	19.1	61.3	68	52.6	23.5	61.8	26.5	27.8	57.3	63.7	14.3	24.6	46.3	31.2	66.8	49.5	44.84

TABLE 5: Quantitative comparison (AP %) on the Pascal VOC 2007 *test* set using a single VGG-16 network. Note that (*) Shi et al. [34] use additional data with BB-level annotation at training time.

Method	aero	bike	bird	boat	bottle	bus	car	cat	chair	cow	table	dog	horse	mbike	persn	plant	sheep	sofa	train	tv	mAP
Cinbis et al. [9]	44.6	42.3	25.5	14.1	11	44.1	36.3	23.2	12.2	26.1	14	29.2	36	54.3	20.7	12.4	26.5	20.3	31.2	23.7	27.4
Li et al. (*) [25]	-	-	-	-	-	-	-	-	-	-	-	-	-	-	-	-	-	-	-	-	21.4
Ours (W_0^P)	55.8	47.5	36.1	16	12.5	46.3	43.7	59.3	11.9	32.2	13.4	41.1	40.3	55.8	8	13	33.8	15.6	42.3	28.5	32.66

TABLE 6: Pascal VOC 2010 *test* set, single AlexNet network. Note that (*) Li et al. [25] use the *val* split for the evaluation. Our results are available at: <http://host.robots.ox.ac.uk:8080/anonymous/WHEGLB.html>.

Method	aero	bike	bird	boat	bottle	bus	car	cat	chair	cow	table	dog	horse	mbike	persn	plant	sheep	sofa	train	tv	mAP
Li et al. (*) [25]	-	-	-	-	-	-	-	-	-	-	-	-	-	-	-	-	-	-	-	-	30.7
Bilen et al. (***) [5]	57.4	51.8	41.2	16.4	22.8	57.3	41.8	34.8	13.1	37.6	10.8	37	45.2	64.9	14.1	22.3	33.8	27.6	49.1	44.8	36.2
Ours (W_0^P)	70.4	60.7	45.7	26	15.6	54.8	54.5	53.7	18.6	42.8	11.2	35.6	53	67	6	21.8	38.3	24.8	60.8	44.2	40.27

TABLE 7: Pascal VOC 2010 *test* set, VGG-16 network. Note that: (*) Li et al. [25] use the *val* split for the evaluation and (**) Bilen et al. [5] use an ensemble of 3 networks: VGG-F [6], VGG-CNN-M-1024 [6] and VGG-16. Our results are available at: <http://host.robots.ox.ac.uk:8080/anonymous/UBLBGP.html>.

iteration’s model. Thus, we remove from Alg. 1 all those steps which concern image (and class) selection. Moreover, we also remove the inter-classifier competition, and we independently select the top score box for each label in Y . More in detail, given $(I, Y) \in T$, for each $y \in Y$ we separately compute:

$$(s_y, z_y) = \arg \max_{\substack{(s_{ic}, p_{ic}) \in f_{W_{t-1}}(I, B(I)), \\ c=y}} s_{ic} \quad (5)$$

Note that Eq. 5 is different from Eq. 2 because only y -specific scores are taken into account. For instance, an image I associated with 3 different labels ($Y = \{y_1, y_2, y_3\}$) will produce 3 corresponding class-specific latent boxes ($\{z_{y_1}, z_{y_2}, z_{y_3}\}$) using Eq. 5 and iterating over $y \in Y$, but at most only one latent box z_y^I using Eq. 2 and the inter-classifier competition constraint (see Sec. 4). In *MIL* we use Eq. 5 to associate each I with the set of its pseudo-ground truth boxes $(I, \{(y, z_y)\}_{y \in Y})$, which are directly added to T_t , skipping Lines 4-12. Note also that Eq. 5 is based on the current network $f_{W_{t-1}}$, including the regression part, which is used at each iteration t to compute the set $\{p_{ic}\}$ over which z_y is selected. Thus, both in *MIL* and in *SP* the bag of boxes associated with I dynamically changes at each iteration t . Finally, note that *MIL* is different from *Init*, since in the latter the pseudo-ground truth is computed only once and using the CN. However, both in *MIL* and in *Init*, $N_t = N = |T|$ is kept fixed in every iteration t and no score-based image selection or class selection is done, hence we use all the images for training.

Curriculum. In contrast, we call *Curriculum* a simplified version of Alg. 1 in which information about “easiness” of images and boxes is given externally to the trained DN. The purpose of this experiment is to show the behaviour of a simplified progressive-image-selection protocol in which image selection is performed “statically” using the scores computed by the CN, as opposed to *SP*, where selection is performed “dynamically” using the current DN $f_{W_{t-1}}$.

In *Curriculum* we use the same pseudo-ground truth used in *Init* and we select images according to the static score values initially computed by the CN. Specifically, we use the boxes and the corresponding scores computed when we build the the training set of *Init* (Sec. 4): For each $(I, Y) \in T$ and for each $y \in Y$, (s_y, z_y) is obtained using Eq. 4 and the CN (h^I and h^P for ILSVRC and Pascal, respectively). Thus, T is the same used in *Init*. However, at each iteration t , T is sorted using the pre-computed scores (s_y) and a subset T_t is extracted from T as in Lines 10-11. When we select T_t we use the same ratio sequence $r_1, \dots, r_t, \dots, r_M$ used in *SP* (see Alg. 1). However, no inter-classifier competition and thus no class-selection is used in *Curriculum*. Images associated with multiple labels are sorted according to their highest score label. Note that in this experiment, despite the values of the latent boxes and their scores are fixed, the model will observe more and more data (from “easy” to “difficult” images) while t increases.

The results are shown in Tab. 8 and 9 for the two datasets, where we report the mAP for different networks f_{W_t} obtained at the end of different iterations t and for each of the training protocols. For all the training procedures $M = 4$ and r_{t+1} is computed as in Line 19 (when it applies). However, in the last column of the table we show the results obtained iterating all the protocols for one more iteration (using $r_{M+1} = 1$). The accuracy impact of the last iteration is generally marginal. The first column of the table (W_0) is the same for all the methods as it is the evaluation of *Init*, which is used as the pre-trained model for all the protocols. The results show that *SP* is able to increase its accuracy during time, confirming the self-paced assumption of a model which progressively becomes more mature and, as a consequence, is more and more reliable when it computes the values of its latent variables.

On the other hand, the other two simplified solutions do not really seem to be able to improve over time. In both datasets *MIL* achieves a final mAP even worse than

Init (both when $t = M$ and when $t = M + 1$). This is probably due to a drifting effect: At time t all the images in T are used for training and a large portion of them are noisy (i.e., are associated with wrong latent boxes). Thus W_t is a weak model and it is used to compute T_{t+1} , most likely producing many errors that will be accumulated over time. In *SP* this problem is alleviated because only the “best” images in T_t are used to train W_t . We do not claim that any MIL-based solution should drift, and, for example, Cinbis et al. [9] combined a standard MIL approach with a multi-fold strategy, observing a progressively increasing accuracy in their experiments. However, the baseline we adopted in our experiments, which is based on the “standard” MIL characteristics (see points (a) and (b) above), embedded in our framework, did not show significant progresses in the two datasets we used for the evaluation, confirming the difficulty of making MIL-like methods work in practice.

On the other hand, sample selection is performed in *Curriculum*, but, similarly to *MIL*, the mAP values oscillate without improving with respect to the starting point. This is probably due to the fact that there can be little progress if the model cannot update the initial predictions done by the CN. Moreover, the sample selection strategy in *SP* takes also into account the inter-classifier competition, prudently discarding those images in which the current model is uncertain, a constraint which is not used in *Curriculum*. In Sec. 7.3 we present another experiment showing the precision of the latent boxes computed by *SP*, which further confirms this hypothesis.

Class selection. In the same tables we show the results of *SP-all-cls*, obtained from *SP* by removing *only* the class-selection part (Lines 6-9) and keeping all the rest unchanged (inter-classifier competition included). In both the datasets *SP-all-cls* achieved a lower final mAP with respect to *SP*, but this is more evident in the case of Pascal. In the latter dataset we performed an additional experiment, called *SP-rnd-cls*, where class selection is performed *randomly*, in such a way that the number of classes (C_t , see Line 7 of Alg. 1) is the same used in *SP* and the results are reported in Tab. 8. *SP-rnd-cls* is able to improve with respect to the initialization but, as expected, the final mAP is much lower than the corresponding mAP obtained with *SP-all-cls*. The reason of this behaviour is most likely due to the fact that, randomly discarding easy classes and the corresponding correct samples, has a negative effect on the final performance. Comparing the category-specific AP obtained with *Init* in ILSVRC with the corresponding AP obtained by *SP* (see Sec. A), 147 classes out of 200 (73.5%) have improved. This demonstrates that the combination of class-selection and inter-classifier competition in *SP* does *not* prevent most of the classes to improve and that the learning process is *not* dominated by few strong classifiers. Finally, we list below the 10 classes selected when $t = 1$ in Pascal in descending order: $S = \{\text{aeroplane, sheep, train, cow, bird, cat, boat, horse, motorbike, car}\}$. As expected, this set includes those “classifiers” which are already strong enough both in h^P and in $f_{W_0^P}$, and it is largely independent of the cardinality of corresponding class samples in T .

Regression. The last part of this ablation study is dedicated to the importance of the regression part. In *SP*, z_y^I is selected over the set $\{p_{ic}\}$, computed using the regression

layer of Fast-RCNN. Choosing z_y^I over the BBs in $B(I)$ at training time but using the regression layer at testing time, we obtain the results reported in Tab. 8 (*No-reg-train*). Note that we can use the regression layer at testing time because the weights of this layer are trained using the pseudo-ground truth, though that layer is not used for selecting z_y^I . Conversely, in *No-reg-train-test* we disable the regression layer also at testing time (in this case f_{W_0} does *not* correspond to *Init*, being the results of *Init* obtained using the regression part). As shown in Tab. 8 there is a large accuracy gap with respect to *SP*. We repeated the *No-reg-train-test* experiment on ILSVRC obtaining a similar very large accuracy gap: a final mAP of 7.57, 4.56 points less than our best result on that dataset. These accuracy differences show the importance of the proposed iterative strategy in which the current network is used to compute the supposed locations of the objects inside the training images.

Method	W_0	W_1	W_2	W_3	W_4	W_5
<i>MIL</i>	31.9	33.6	32.1	32.2	30.8	30.9
<i>Curriculum</i>	31.9	31.3	33.8	31.6	31.3	30.5
<i>SP-all-cls</i>	31.9	36.6	36.9	36.6	36.9	36.9
<i>SP-rnd-cls</i>	31.9	32.3	31.6	32.4	32.7	33.8
<i>No-reg-train</i>	31.9	31.2	32.6	33.1	33.5	34.4
<i>No-reg-train-test</i>	28.3	28.3	30.1	30.9	30.7	31.4
<i>SP</i>	31.9	35.3	37.6	37.8	38.1	38.1

TABLE 8: mAP (%) on Pascal VOC 2007 *test* computed with different networks f_{W_t} and with respect to different versions of our training protocol and $M + 1$ iterations.

Method	W_0	W_1	W_2	W_3	W_4	W_5
<i>MIL</i>	9.54	9.66	9.01	8.97	8.59	8.7
<i>Curriculum</i>	9.54	9.08	9.15	8.77	8.89	8.97
<i>SP-all-cls</i>	9.54	10.68	10.74	11.77	11.97	12.06
<i>SP</i>	9.54	10.88	11.87	12.01	12.13	11.87

TABLE 9: mAP (%) on ILSVRC 2013 *val2* computed with different networks f_{W_t} and with respect to different versions of our training protocol and $M + 1$ iterations.

7.2 Multi-label versions of the training protocol

This subsection is dedicated to evaluating the importance of the inter-classifier competition. As explained in Sec. 4 the inter-classifier competition is used in *SP* to reduce the amount of noisy training boxes by selecting only one box z_y^I per image I , according to the current most confident classifier (y) on I . A disadvantage of this strategy is the sacrifice of possible other “good” boxes associated with either other classes ($y' \neq y, y' \in Y$) or the same class. For instance, the latter situation occurs when more than one instance of the category *person* is contained in I (recall that we only know that $person \in Y$, without any information about the cardinality of the instances for each image). We report below our study of two different versions of *SP*: *SP-SIML* and *SP-MIML*, where we relax the inter-classifier competition for a multiple-label and a multiple-instance scenario.

Multiple-label. *SP-SIML* is a Single-Instance-Multiple-Label version of Alg. 1, where in each image we mine one

box *per each label* in Y . Similarly to *MIL*, given $(I, Y) \in T$, for each $y \in Y$ we use Eq. 5 to compute a set of candidate boxes associated with I : $P_I = (I, \{(s_y, z_y, y)\}_{y \in Y})$. However, before adding P_I to P , in Line 5 we remove from P_I those boxes which have a score lower than the top-score box of all the other categories $\bar{Y} = \{1, \dots, C\} \setminus Y$. \bar{Y} is the complement of Y (it contains the set of all the labels *not* included in Y) and it is used to compute s_y^o :

$$(s_y^o, z_y^o) = \arg \max_{(s_{ic}, p_{ic}) \in f_{W_{t-1}}(I, B(I)), c \in \bar{Y}} s_{ic} \quad (6)$$

The value s_y^o is used to prune from P_I all those elements whose score s_y is lower than s_y^o . The intuitive idea behind this procedure is that we relax the inter-classifier competition, collecting more boxes in those images associated with multiple labels (there is no competition among classes contained in Y). However, we impose that a classifier for class y , $y \in Y$, should be more confident than the strongest *noisy* classifier firing on z_y^o . Note also that we do not need to modify the class-selection strategy because $e(c)$ (Line 6) can be computed using Eq. 3 which applies also to the case in which a given image $I \in P$ is associated with multiple boxes. Intuitively, in *SP-SIML*, both the class selection and intra-image box pruning are based on the competition between classifiers in Y and classifiers in \bar{Y} . Apart from Lines 3-5, modified as explained above, *SP-SIML* is identical to *SP*, including score-based image selection.

Multiple-label and multiple-instance. *SP-MIML* is a Multiple-Instance-Multiple-Label extension of *SP-SIML*, where more than one box of the same category $y \in Y$ can be collected from the same image I . *SP-MIML* is obtained applying standard Non-Maxima Suppression (NMS) over $f_{W_{t-1}}(I, B(I))$ and then, for each $y \in Y$, keeping all those boxes whose value is higher than s_y^o (thus, no ad hoc, manually tuned threshold on the box scores after NMS needs to be used). Also in this case, we use both score-based image selection (Lines 10-11) and class-selection and we modify only Lines 3-5 in Alg. 1 to obtain *SP-MIML*.

We test *SP-SIML* and *SP-MIML* on Pascal VOC 2007 because Pascal VOC images contain more objects and more labels on average with respect to ILSVRC 2013. In Tab. 10 we show the results which have been obtained using W_0^P as the initialization and using the same hyper-parameter values used in the other experiments (see Sec. 4).

Method	mAP
<i>SP-SIML</i>	33.80
<i>SP-MIML</i>	34.43
<i>SP</i>	38.11

TABLE 10: Results (mAP %) on the Pascal VOC 2007 *test* set using relaxed versions of the inter-classifier competition.

Unexpectedly, *SP* largely outperforms both *SP-SIML* and *SP-MIML*, despite more data are used in the latter two versions (because more boxes on average are collected from a single image I). Our interpretation of this result is that the inter-classifier competition is very important for a prudent choice of the latent boxes, forcing the system to select a box z_y^I only when its classification confidence s_y^I is very

high. To confirm this hypothesis, we computed the average CorLoc over all the self-paced iterations and using *SP*, *SP-SIML* and *SP-MIML*. Consistently in all $M = 4$ iterations the CorLoc of both *SP-SIML* and *SP-MIML* is much smaller than the corresponding values obtained with *SP*, which means that the mined pseudo-ground truth is less precise. A visual inspection of randomly selected images further confirmed that most of the times the additional boxes selected in both *SP-SIML* and *SP-MIML* with respect to z_y^I are inaccurately localized or completely wrong. However, although the multi-label extensions of *SP* underperformed with respect to *SP*, their final mAP is comparable with the state of the art on Pascal VOC 07 (see Tab. 2).

7.3 Precision of the selected subsets of training data

In this subsection we evaluate the number of “correct” samples selected for training the network. To this aim we adopt the evaluation protocol suggested in [17], where the authors use ILSVRC 2013 *val1* and a Precision metric. The latter is similar to CorLoc, the difference being that in CorLoc one latent box (z_y) is computed for each label $y \in Y$ associated with a training image, while Precision is based on extracting one single latent box (z_y^I) per image. Using Precision @0.5 IoU we can measure the quantity of latent boxes actually used during training which sufficiently overlap with a real ground truth box with the correct class.

In Tab. 11 we show the results, where *Precision* is the percentage of correct image samples over all the images included in the training set T_t . In case of [17], Precision is computed with respect to the whole *val1* because no subset selection is done in that work. T_1 in Tab. 11 is the dataset obtained with the initialization model W_0 and used to train W_1 , while T_4 is the dataset obtained with W_3 and used in the last iteration to train W_4 . As shown in the table, Precision in T_4 is largely improved with respect to Precision in T_1 . Precision in T_4 is much higher than the Precision obtained by [17], even when *object-level* annotation for 100 over 200 categories is used as auxiliary data during training.

In Fig. 3-4 we show the evolution of the class-specific top-score box z_y for the same image I over the four self-paced iterations. The new localizations usually improve with respect to the previous ones.

8 CONCLUSIONS

We proposed a self-paced learning based protocol for deep networks in a WSD scenario, aiming at reducing the amount of noise while training the DN. Our training protocol extends the self-paced learning paradigm by introducing: (1) inter-classifier competition as a powerful mechanism to reduce noise, (2) class-selection, in which the easiest classes are trained first, and (3) the use of the Fast-RCNN regression layer for the implicit modification of the bag of boxes.

While in the past self-paced learning strategies have been successfully adopted for other classifier types (mainly SVMs), we are the first showing that this paradigm can be successfully utilized also for an end-to-end training of deep networks. Despite the reduced sizes of the initial training subsets, typical in a self-paced strategy, we have empirically shown that our training protocol not only does not suffer

Method	Precision (IoU > 0.5)
Hoffman et al. [17] without auxiliary strongly supervised data	26.10
Hoffman et al. [17] with auxiliary strongly supervised data	28.81
$SP(T_1)$	20.55
$SP(T_4)$	37.01

TABLE 11: Precision of the selected boxes used for training. In SP the Precision value is computed over the elements in T_t , which is a subset of ILSVRC 2013 *val1*, while in [17] Precision is computed over the whole *val1*. However, the comparison is fair because, differently from [17], we do *not* use the whole *val1* for training but only the subset T_t , thus the quality of the training boxes should be compared with only those samples actually used for training.

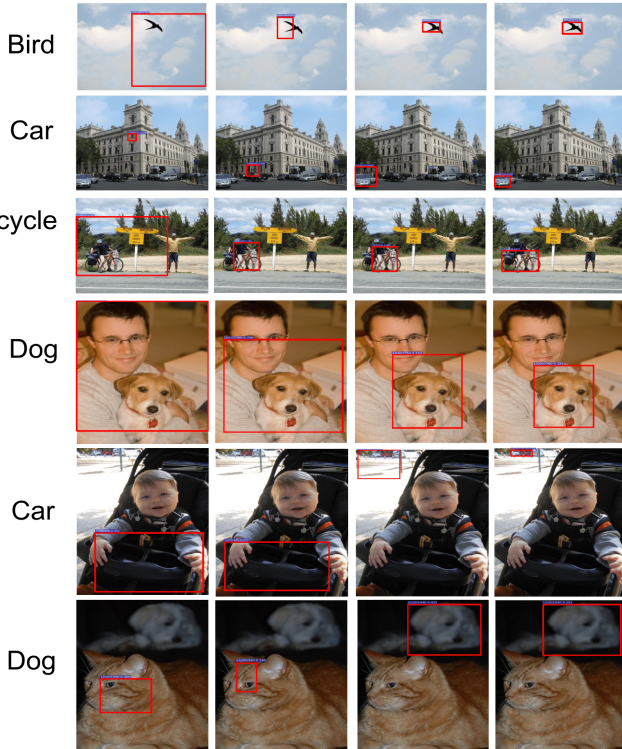


Fig. 3. Qualitative results: visualizations of the class-specific top-score box z_y in the four self-paced iterations (chronologically ordered from left to right) with respect to different training images and labels y (leftmost column).

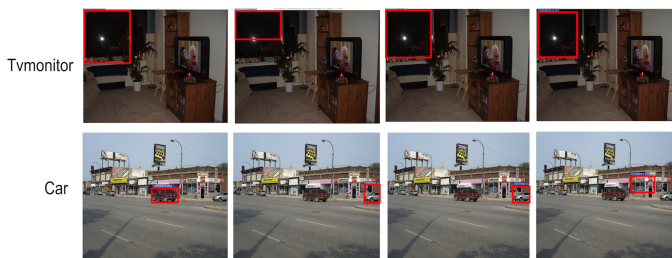


Fig. 4. Other qualitative results in which the evolution over time of the class-specific top-score box (z_y) of the network did *not* succeed in localizing the true objects into the images.

for overfitting, but it benefits from the reduced noise, by largely boosting the final accuracy with respect to different initialization methods.

Using the proposed training protocol we achieved state-of-the-art results on common WSD benchmarks: ILSVRC 2013, Pascal VOC 2007 and VOC 2010.

Finally, we presented a detailed analysis of the main components of our proposed training protocol, comparing SP with both simplified and more sophisticated versions of the same approach, with the goal of showing the importance of our design choices and to allow other authors to build on our method, possibly choosing those components which best fit with other application scenarios.

ACKNOWLEDGEMENTS

We want to thank the NVIDIA Corporation for the donation of the GPUs used in this project.

REFERENCES

- [1] L. Bazzani, A. Bergamo, D. Anguelov, and L. Torresani. Self-taught object localization with deep networks. In *IEEE Winter Conference on Applications of Computer Vision (WACV)*, 2016.
- [2] Y. Bengio, J. Louradour, R. Collobert, and J. Weston. Curriculum learning. In *ICML*, pages 41–48, 2009.
- [3] H. Bilen, M. Pedersoli, and T. Tuytelaars. Weakly supervised object detection with posterior regularization. In *BMVC*, 2014.
- [4] H. Bilen, M. Pedersoli, and T. Tuytelaars. Weakly supervised object detection with convex clustering. In *CVPR*, 2015.
- [5] H. Bilen and A. Vedaldi. Weakly supervised deep detection networks. In *CVPR*, 2016.
- [6] K. Chatfield, K. Simonyan, A. Vedaldi, and A. Zisserman. Return of the devil in the details: Delving deep into convolutional nets. In *BMVC*, 2014.
- [7] X. Chen and A. Gupta. Webly supervised learning of convolutional networks. In *ICCV*, 2015.
- [8] R. G. Cinbis, J. J. Verbeek, and C. Schmid. Multi-fold MIL training for weakly supervised object localization. In *CVPR*, pages 2409–2416, 2014.
- [9] R. G. Cinbis, J. J. Verbeek, and C. Schmid. Weakly supervised object localization with multi-fold multiple instance learning. *IEEE Trans. Pattern Anal. Mach. Intell.*, 39(1):189–203, 2017.
- [10] M. Everingham, L. Van Gool, C. K. Williams, J. Winn, and A. Zisserman. The Pascal Visual Object Classes Challenge 2007 (VOC 2007) Results.
- [11] M. Everingham, L. Van Gool, C. K. Williams, J. Winn, and A. Zisserman. The Pascal Visual Object Classes (VOC) challenge. *IJCV*, 88(2):303–338, 2010.
- [12] R. B. Girshick. Fast R-CNN. In *ICCV*, 2015.
- [13] R. B. Girshick, J. Donahue, T. Darrell, and J. Malik. Rich feature hierarchies for accurate object detection and semantic segmentation. In *CVPR*, 2014.
- [14] G. Gkioxari, R. B. Girshick, and J. Malik. Contextual action recognition with R*CNN. In *ICCV*, 2015.
- [15] K. He, G. Gkioxari, P. Dollár, and R. B. Girshick. Mask R-CNN. In *ICCV*, 2017.
- [16] J. Hoffman, S. Guadarrama, E. Tzeng, R. Hu, J. Donahue, R. B. Girshick, T. Darrell, and K. Saenko. LSDA: large scale detection through adaptation. In *NIPS*, 2014.

- [17] J. Hoffman, D. Pathak, T. Darrell, and K. Saenko. Detector discovery in the wild: Joint multiple instance and representation learning. In *CVPR*, pages 2883–2891, 2015.
- [18] L. Jiang, D. Meng, S. Yu, Z. Lan, S. Shan, and A. G. Hauptmann. Self-paced learning with diversity. In *NIPS*, pages 2078–2086, 2014.
- [19] V. Kantorov, M. Oquab, M. Cho, and I. Laptev. ContextLocNet: context-aware deep network models for weakly supervised localization. In *ECCV*, 2016.
- [20] A. Khosla, T. Zhou, T. Malisiewicz, A. Efros, and A. Torralba. Undoing the damage of dataset bias. In *ECCV*, 2012.
- [21] A. Krizhevsky, I. Sutskever, and G. E. Hinton. ImageNet classification with deep convolutional neural networks. In *NIPS*, 2012.
- [22] M. P. Kumar, B. Packer, and D. Koller. Self-paced learning for latent variable models. In *NIPS*, pages 1189–1197, 2010.
- [23] Á. Lapedriza, H. Pirsiavash, Z. Bylinskii, and A. Torralba. Are all training examples equally valuable? *arxiv:1311.6510*, 2013.
- [24] Y. J. Lee and K. Grauman. Learning the easy things first: Self-paced visual category discovery. In *CVPR*, pages 1721–1728, 2011.
- [25] D. Li, J.-B. Huang, Y. Li, S. Wang, and M.-H. Yang. Weakly supervised object localization with progressive domain adaptation. In *CVPR*, 2016.
- [26] X. Liang, S. Liu, Y. Wei, L. Liu, L. Lin, and S. Yan. Towards computational baby learning: A weakly-supervised approach for object detection. In *ICCV*, 2015.
- [27] T. Malisiewicz, A. Gupta, and A. A. Efros. Ensemble of Exemplar-SVMs for object detection and beyond. In *ICCV*, 2011.
- [28] M. H. Nguyen, L. Torresani, F. D. la Torre, and C. Rother. Learning discriminative localization from weakly labeled data. *Pattern Recognition*, 47(3):1523–1534, 2014.
- [29] M. Oquab, L. Bottou, I. Laptev, and J. Sivic. Is object localization for free? - Weakly-supervised learning with convolutional neural networks. In *CVPR*, pages 685–694, 2015.
- [30] A. Pentina, V. Sharmanska, and C. H. Lampert. Curriculum learning of multiple tasks. In *CVPR*, pages 5492–5500, 2015.
- [31] O. Russakovsky, J. Deng, H. Su, J. Krause, S. Satheesh, S. Ma, Z. Huang, A. Karpathy, A. Khosla, M. S. Bernstein, A. C. Berg, and F. Li. Imagenet large scale visual recognition challenge. *arxiv:1409.0575*, 2014.
- [32] E. Sangineto. Statistical and spatial consensus collection for detector adaptation. In *ECCV*, pages 456–471, 2014.
- [33] F. Schroff, D. Kalenichenko, and J. Philbin. FaceNet: A unified embedding for face recognition and clustering. In *CVPR*, pages 815–823, 2015.
- [34] M. Shi and V. Ferrari. Weakly supervised object localization using size estimates. In *ECCV*, pages 105–121, 2016.
- [35] A. Shrivastava, A. Gupta, and R. Girshick. Training region-based object detectors with online hard example mining. In *CVPR*, 2016.
- [36] K. Simonyan and A. Zisserman. Very deep convolutional networks for large-scale image recognition. *arXiv:1409.1556*, 2014.
- [37] H. O. Song, R. Girshick, S. Jegelka, J. Mairal, Z. Harchaoui, and T. Darrell. On learning to localize objects with minimal supervision. In *ICML*, 2014.
- [38] H. O. Song, Y. J. Lee, S. Jegelka, and T. Darrell. Weakly-supervised discovery of visual pattern configurations. In *NIPS*, 2014.
- [39] J. S. Supancic III and D. Ramanan. Self-paced learning for long-term tracking. In *CVPR*, pages 2379–2386, 2013.
- [40] E. W. Teh, M. Rochan, and Y. Wang. Attention networks for weakly supervised object localization. In *BMVC*, 2016.
- [41] J. R. R. Uijlings, K. E. A. van de Sande, T. Gevers, and A. W. M. Smeulders. Selective search for object recognition. *International Journal of Computer Vision*, 104(2):154–171, 2013.
- [42] C. Wang, K. Huang, W. Ren, J. Zhang, and S. J. Maybank. Large-scale weakly supervised object localization via latent category learning. *IEEE Transactions on Image Processing*, 24(4):1371–1385, 2015.
- [43] Y. Wei, X. Liang, Y. Chen, X. Shen, M. Cheng, J. Feng, Y. Zhao, and S. Yan. STC: A simple to complex framework for weakly-supervised semantic segmentation. *IEEE Trans. Pattern Anal. Mach. Intell.*, 39(11):2314–2320, 2017.
- [44] W. Zaremba and I. Sutskever. Learning to execute. *arXiv:1410.4615*, 2014.
- [45] D. Zhang, D. Meng, L. Zhao, and J. Han. Bridging saliency detection to weakly supervised object detection based on self-paced curriculum learning. In *IJCAI*, pages 3538–3544, 2016.



Enver Sangineto is a research fellow at University of Trento, Department of Information Engineering and Computer Science. He received his PhD in Computer Engineering from the University of Rome “La Sapienza”. After that he has been a post-doctoral researcher at “La Sapienza” and at the Italian Institute of Technology in Genova. His research interests include object detection and learning with minimal human supervision.



Moin Nabi is a Senior Research Scientist at SAP Machine Learning Research in Berlin. Before that, he was a postdoctoral research fellow in the Deep Relational Learning group at the University of Trento and a visiting researcher in the GRAIL lab at the University of Washington. He holds a PhD from the Italian Institute of Technology. His research lies at the intersection of machine learning, computer vision, and natural language processing with an emphasis on learning Deep Neural Networks with minimal supervision and/or limited data.



Dubravko Culibrk is a Professor at the University of Novi Sad, Serbia and the director of the Industry/University Center for Collaborative Research of the Faculty of Technical Sciences. His interests are in the domain of computer vision, machine learning and knowledge discovery. Prof. Culibrk received his B.Eng. degree in Electrical Engineering and an M.Sc. degree in Computer Engineering from the University of Novi Sad, Serbia, in 2000 and 2003, respectively, as well as a Ph.D. degree in computer engineering from Florida Atlantic University, Boca Raton, USA, in 2006.



Nicu Sebe is Professor with the University of Trento, Italy, leading the research in the areas of multimedia information retrieval and human behavior understanding. He was the General Chair of the IEEE FG Conference 2008, ACM Multimedia 2013 and ICMR 2017, and the Program Chair of the International Conference on Image and Video Retrieval in 2007 and 2010, ACM Multimedia 2007 and 2011, ECCV 2016 and ICCV 2017. He is the Program Chair of ICPR 2020. He is a fellow of the International Association for

APPENDIX

In Tab. 12 we show the per-category AP obtained by our method on ILSVRC 2013 *val2*. Similarly to Sec. 7.1, we analyse 5 different nets (W_0, \dots, W_4), corresponding to the 4 self-paced iterations of Alg. 1 plus the initialization model ($W_0 = W_0^I$, i.e., *Init*), used as a comparison. This is done in order to show that most of the categories progressively improve during training and that this improvement is generalized and not dominated by a few categories. In fact, the AP of 147 out of 200 categories increases when evaluated using f_{W_4} with respect to the evaluation obtained using the initial model f_{W_0} (see Sec. 7.1).

This is not a trivial result, because the combination of class-selection and inter-classifier competition in *SP* could potentially lead the sample selection process to be dominated by a few strong categories in f_{W_0} . For instance, categories like antelope or fox, which have AP 22.09 and 22.61 using f_{W_0} , respectively, are already strong in the beginning of the learning process and could dominate the selection of new samples in T_1, T_2, \dots . Conversely, initially very weak classifiers like cream or oboe (AP 3.06 and 1.51 using f_{W_0} , respectively) could be penalized because not able to win the inter-classifier competition or because excluded by the class-selection process. However, our empirical results show that this harmful domination of the initial strong classifiers does *not* happen and that learning is spread over most of the categories. We believe that this is due to the fact that good classifiers (e.g., antelope) do *not* have high scores in an image showing an oboe, because most of the BBs of the oboe's image (background boxes included) have an appearance different from an antelope. Thus even a weak classifier can win the competition on its own samples and "gain" new samples to add to the next training set T_t which will finally lead to the improvement the weak classifier.

#	Category	W0	W1	W2	W3	W4
1	accordion	31.83	31.50	32.31	27.45	33.25
2	airplane	34.55	32.93	35.55	43.35	42.61
3	ant	17.79	15.58	16.75	15.77	16.14
4	antelope	22.09	24.85	30.44	32.61	31.36
5	apple	6.07	10.32	10.54	10.96	11.48
6	armadillo	32.39	32.16	33.95	37.25	37.49
7	artichoke	14.85	15.03	17.03	18.28	18.22
8	axe	0.80	0.10	1.15	2.47	1.47
9	baby bed	4.65	17.66	19.40	18.44	14.33
10	backpack	1.39	1.69	1.90	2.26	2.06
11	bagel	6.11	10.32	11.64	11.57	11.81
12	balance beam	0.03	0.12	0.15	0.20	0.19
13	banana	7.13	6.78	8.73	8.82	13.67
14	band aid	0.27	3.52	0.41	0.48	0.62
15	banjo	18.92	11.32	11.18	6.22	6.29
16	baseball	7.21	18.38	23.41	27.91	27.90
17	basketball	0.00	0.01	0.00	0.00	0.00
18	bathing cap	2.38	4.89	2.44	1.40	1.48
19	beaker	4.17	10.02	10.83	11.70	11.20
20	bear	31.87	29.54	31.77	28.81	29.42
21	bee	12.85	15.61	15.85	14.04	19.51
22	bell pepper	9.21	11.48	7.92	8.84	8.71
23	bench	1.82	3.26	1.07	0.52	0.59
24	bicycle	19.05	21.71	21.87	22.05	21.43
25	binder	3.83	3.31	4.28	4.38	4.90
26	bird	39.59	43.81	47.81	47.24	46.97
27	bookshelf	4.92	7.76	9.55	7.62	7.68
28	bow	0.89	1.10	1.79	1.24	1.20
29	bow tie	0.23	0.12	0.10	1.88	1.49
30	bowl	5.08	5.37	6.29	8.40	7.58
31	brassiere	9.01	10.68	11.26	11.18	11.67
32	burrito	3.03	2.16	5.01	5.00	5.33
33	bus	28.70	37.36	36.12	36.26	34.82
34	butterfly	60.85	60.18	67.47	67.87	67.47
35	camel	6.66	7.92	9.59	10.65	10.33
36	can opener	8.48	11.41	12.15	10.64	12.79
37	car	21.11	22.33	22.98	24.82	25.07
38	cart	12.62	11.46	11.52	11.68	11.01
39	cattle	9.97	3.35	6.24	5.39	6.27
40	cello	6.49	12.75	13.70	16.99	16.92
41	centipede	13.34	12.75	16.59	16.26	19.86
42	chain saw	0.09	0.70	2.08	1.80	2.17
43	chair	4.03	5.13	6.10	5.60	5.53
44	chime	6.94	10.43	7.81	3.31	6.34
45	cocktail shaker	11.75	10.23	13.56	14.93	15.37
46	coffee maker	3.31	12.70	12.36	15.27	11.37
47	computer keyboard	3.18	5.89	9.20	11.36	11.78
48	computer mouse	1.70	1.71	1.71	2.78	2.21
49	corkscrew	13.03	9.63	10.76	13.17	13.06
50	cream	3.06	5.61	6.80	10.82	10.65

TABLE 12: Per-class AP on the ILSVRC13 detection *val2*.

#	Category	W0	W1	W2	W3	W4
51	croquet ball	1.72	0.66	0.28	0.16	0.25
52	crutch	1.34	1.96	1.79	1.85	2.78
53	cucumber	5.22	4.52	3.59	3.65	3.41
54	cup or mug	7.51	7.28	11.99	12.10	12.67
55	diaper	1.46	4.60	3.13	3.43	2.96
56	digital clock	4.62	13.05	20.51	19.04	19.35
57	dishwasher	7.79	0.79	0.96	0.70	0.67
58	dog	16.80	15.59	17.34	19.32	17.35
59	domestic cat	4.10	3.87	3.15	4.87	3.23
60	dragonfly	18.44	16.02	26.51	25.22	25.29
61	drum	0.23	0.42	0.57	0.56	0.57
62	dumbbell	2.56	1.49	1.43	1.32	1.36
63	electric fan	28.65	16.71	16.83	20.57	21.10
64	elephant	31.17	38.46	34.92	37.21	34.44
65	face powder	9.96	7.85	6.27	5.19	4.65
66	fig	7.56	7.69	6.70	4.59	4.10
67	filig cabinet	3.60	6.26	7.72	6.92	7.74
68	flower pot	0.24	0.39	0.28	0.27	0.27
69	flute	0.08	1.68	1.67	1.60	1.57
70	fox	22.61	28.19	28.73	32.96	36.23
71	french horn	9.17	10.71	10.50	16.79	12.28
72	frog	22.53	28.31	29.88	29.37	30.08
73	frying pan	5.08	4.03	4.41	5.79	5.70
74	giant panda	34.60	46.05	46.31	26.62	26.71
75	goldfish	5.37	9.75	7.69	9.40	9.42
76	golf ball	17.15	22.84	23.18	23.10	22.91
77	golfcart	32.61	24.31	28.82	31.24	33.59
78	guacamole	13.27	8.80	8.33	8.65	8.28
79	guitar	5.49	5.35	6.69	4.91	4.82
80	hair dryer	3.74	0.44	0.86	1.36	1.28
81	hair spray	1.71	2.57	3.85	3.75	4.94
82	hamburger	15.57	31.05	25.96	17.97	17.92
83	hammer	0.72	0.54	0.64	1.27	1.58
84	hamster	41.87	31.78	42.78	39.35	39.29
85	harmonica	0.49	0.94	0.76	0.62	0.50
86	harp	21.65	30.85	34.71	38.22	37.95
87	hat with a wide brim	6.10	10.00	11.51	9.85	11.37
88	head cabbage	4.92	8.11	8.76	9.63	9.64
89	helmet	5.08	4.10	4.51	5.16	5.43
90	hippopotamus	21.24	24.43	30.54	27.03	27.58
91	horizontal bar	0.04	0.07	0.07	0.05	0.05
92	horse	7.34	6.74	9.30	9.06	8.90
93	hotdog	4.06	4.74	4.12	4.13	3.77
94	iPod	15.80	26.91	26.39	25.08	25.70
95	isopod	10.06	13.45	12.88	13.31	10.11
96	jellyfish	7.32	3.41	2.76	4.39	4.36
97	koala bear	37.38	46.53	50.72	56.96	52.95
98	ladle	0.47	1.75	0.52	0.57	0.58
99	ladybug	11.74	13.94	13.06	13.69	13.35
100	lamp	0.99	0.87	0.61	0.53	0.58

#	Category	W0	W1	W2	W3	W4
101	laptop	7.60	14.38	15.47	18.66	18.75
102	lemon	5.81	10.57	14.28	14.60	15.03
103	lion	4.51	0.80	2.56	2.04	1.90
104	lipstick	3.50	3.74	3.14	4.04	3.85
105	lizard	6.39	11.37	13.14	13.30	13.78
106	lobster	5.12	8.48	17.80	19.80	15.46
107	maillot	0.20	1.64	1.35	1.05	1.36
108	maraca	3.36	2.65	1.53	1.57	1.55
109	microphone	0.07	0.03	0.06	0.10	0.11
110	microwave	19.30	18.18	14.61	14.25	14.32
111	milk can	16.62	19.41	21.39	14.75	17.97
112	miniskirt	0.74	0.89	0.48	0.19	0.20
113	monkey	17.49	18.81	24.26	26.50	24.46
114	motorcycle	19.21	19.08	26.79	26.96	26.70
115	mushroom	13.53	16.11	17.66	18.54	18.66
116	nail	0.07	0.44	0.21	0.13	0.19
117	neck brace	0.11	6.26	1.29	0.21	0.20
118	oboe	1.51	7.16	7.52	7.47	7.51
119	orange	3.85	1.69	5.58	6.42	6.14
120	otter	2.73	2.19	5.89	8.51	9.02
121	pencil box	2.89	6.76	6.25	4.28	4.84
122	pencil sharpener	1.49	2.35	2.05	1.42	1.59
123	perfume	11.55	2.33	5.54	5.09	5.48
124	person	0.14	0.27	0.37	0.47	0.47
125	piano	5.06	3.21	9.26	11.43	11.45
126	pineapple	6.20	12.69	12.49	11.82	11.92
127	ping-pong ball	0.01	0.01	0.01	0.01	0.01
128	pitcher	3.66	5.98	7.53	8.35	8.08
129	pizza	8.89	17.77	14.55	11.71	11.55
130	plastic bag	0.39	2.21	2.74	2.82	2.55
131	plate rack	1.78	1.08	2.62	6.29	6.19
132	pomegranate	8.72	8.89	9.15	9.24	9.42
133	popsicle	0.06	0.04	0.01	0.01	0.01
134	porcupine	24.08	26.20	33.64	29.51	31.30
135	power drill	0.83	1.01	5.40	7.14	7.10
136	pretzel	3.33	4.79	6.04	6.20	6.40
137	printer	6.17	2.79	2.37	2.42	2.29
138	puck	0.01	0.01	0.01	0.01	0.01
139	punching bag	0.58	2.33	3.65	4.35	4.03
140	purse	0.82	1.23	1.32	1.28	1.29
141	rabbit	43.34	48.27	47.09	48.31	48.41
142	racket	0.05	0.06	0.08	0.08	0.06
143	ray	10.26	14.08	19.76	20.22	22.67
144	red panda	16.13	27.36	22.34	25.36	25.28
145	refrigerator	9.90	10.05	8.14	9.21	8.13
146	remote control	17.05	26.71	32.35	24.36	25.56
147	rubber eraser	0.01	0.01	0.01	0.01	0.01
148	rugby ball	0.04	0.06	0.05	0.04	0.04
149	ruler	0.30	1.89	3.84	3.66	3.90
150	salt or pepper shaker	9.99	8.50	7.69	5.45	6.92

#	Category	W0	W1	W2	W3	W4
151	saxophone	15.90	14.08	13.23	11.66	12.78
152	scorpion	15.23	17.18	22.04	18.47	16.83
153	screwdriver	0.11	0.17	0.13	0.68	0.35
154	seal	2.22	3.18	3.33	3.30	3.96
155	sheep	18.81	14.57	18.88	19.25	18.59
156	ski	0.09	0.02	0.14	0.06	0.06
157	skunk	6.61	9.70	9.19	12.30	10.85
158	snail	24.51	11.68	16.11	19.22	19.46
159	snake	1.58	5.20	12.69	15.81	16.05
160	snowmobile	21.22	31.10	27.13	25.74	28.05
161	snowplow	33.11	38.49	37.20	41.74	41.12
162	soap dispenser	0.01	0.50	0.19	0.20	0.17
163	soccer ball	20.17	19.04	17.84	18.06	18.04
164	sofa	7.65	8.22	7.14	7.66	7.71
165	spatula	0.04	0.04	0.07	0.11	0.12
166	squirrel	17.91	10.72	16.12	25.52	23.18
167	starfish	3.88	9.89	13.17	17.33	17.25
168	stethoscope	2.12	2.97	7.39	7.67	7.74
169	stove	0.58	1.32	1.81	2.18	2.04
170	strainer	0.14	0.26	0.87	3.64	3.76
171	strawberry	4.90	7.82	7.52	7.33	7.20
172	stretcher	0.10	0.01	0.15	0.10	0.10
173	sunglasses	1.51	2.52	1.39	1.35	1.74
174	swimming trunks	0.11	0.03	0.00	0.00	0.00
175	swine	18.70	23.02	28.07	34.95	31.21
176	syringe	1.55	2.62	2.64	2.64	2.62
177	table	1.36	3.18	3.77	3.25	3.34
178	tape player	11.73	8.12	8.94	9.92	10.32
179	tennis ball	8.88	7.11	1.61	1.75	1.35
180	tick	19.72	18.95	24.49	17.99	18.74
181	tie	3.13	2.91	3.43	2.25	3.28
182	tiger	10.38	15.88	18.89	20.83	26.02
183	toaster	22.46	22.21	21.94	21.79	22.69
184	traffic light	1.20	1.14	1.03	0.82	0.90
185	train	10.28	22.47	19.73	17.29	17.68
186	trombone	3.49	4.04	1.15	1.72	1.66
187	trumpet	2.66	4.12	3.75	3.83	3.88
188	turtle	22.47	27.24	31.95	31.68	32.04
189	tv or monitor	20.12	29.23	33.18	33.81	33.84
190	unicycle	0.96	1.51	0.70	0.54	0.56
191	vacuum	1.49	0.50	0.48	0.67	0.37
192	violin	2.02	2.06	3.19	2.42	5.22
193	volleyball	0.02	0.09	0.02	0.02	0.02
194	waffle iron	2.71	2.03	2.29	2.98	4.09
195	washer	41.19	35.88	34.47	30.45	31.32
196	water bottle	5.28	7.32	4.89	6.23	6.05
197	watercraft	6.62	6.55	5.68	3.65	4.39
198	whale	23.15	27.97	32.27	33.57	37.38
199	wine bottle	2.74	1.75	1.87	1.34	1.74
200	zebra	31.42	42.00	43.26	40.14	42.17
—	mAP	9.54	10.88	11.87	12.01	12.13

Self Paced Deep Learning for Weakly Supervised Object Detection - Supplemental Material

Enver Sangineto[†], Moin Nabi[†], Dubravko Culibrk and Nicu Sebe,

In Tab. I we show the per-category AP obtained by our method on ILSVRC 2013 *val2*. Similarly to Sec. 7.1 of the main paper, we analyse 5 different nets (W_0, \dots, W_4), corresponding to the 4 self-paced iterations of Alg. 1 plus the initialization model ($W_0 = W_0^I$, i.e., *Init*), used as a comparison. This is done in order to show that most of the categories progressively improve during training and that this improvement is generalized and not dominated by a few categories. In fact, as mentioned in the main paper, the AP of 147 out of 200 categories increases when evaluated using f_{W_4} with respect to the evaluation obtained using the initial model f_{W_0} (see Sec. 7.1 of the main paper).

This is not a trivial result, because the combination of class-selection and inter-classifier competition in *SP* could potentially lead the sample selection process to be dominated by a few strong categories in f_{W_0} . For instance, categories like antelope or fox, which have AP 22.09 and 22.61 using f_{W_0} , respectively, are already strong in the beginning of the learning process and could dominate the selection of new samples in T_1, T_2, \dots . Conversely, initially very weak classifiers like cream or oboe (AP 3.06 and 1.51 using f_{W_0} , respectively) could be penalized because not able to win the inter-classifier competition or because excluded by the class-selection process. However, our empirical results show that this harmful domination of the initial strong classifiers does *not* happen and that learning is spread over most of the categories. We believe that this is due to the fact that good classifiers (e.g., antelope) do *not* have high scores in an image showing an oboe, because most of the BBs of the oboe's image (background boxes included) have an appearance different from an antelope. Thus even a weak classifier can win the competition on its own samples and "gain" new samples to add to the next training set T_t which will finally lead to the improvement of the weak classifier.

E. Sangineto, Moin Nabi and Nicu Sebe are with the Department of Information Engineering and Computer Science (DISI), University of Trento, Italy.
 E-mail: {enver.sangineto,moin.nabi}@unitn.it; sebe@disi.unitn.it

D. Culibrk is with the Department of Industrial Engineering and Management, University of Novi Sad, Serbia.
 E-mail: dculibrk@uns.ac.rs

[†] These two authors contributed equally.

#	Category	W0	W1	W2	W3	W4
1	accordion	31.83	31.50	32.31	27.45	33.25
2	airplane	34.55	32.93	35.55	43.35	42.61
3	ant	17.79	15.58	16.75	15.77	16.14
4	antelope	22.09	24.85	30.44	32.61	31.36
5	apple	6.07	10.32	10.54	10.96	11.48
6	armadillo	32.39	32.16	33.95	37.25	37.49
7	artichoke	14.85	15.03	17.03	18.28	18.22
8	axe	0.80	0.10	1.15	2.47	1.47
9	baby bed	4.65	17.66	19.40	18.44	14.33
10	backpack	1.39	1.69	1.90	2.26	2.06
11	bagel	6.11	10.32	11.64	11.57	11.81
12	balance beam	0.03	0.12	0.15	0.20	0.19
13	banana	7.13	6.78	8.73	8.82	13.67
14	band aid	0.27	3.52	0.41	0.48	0.62
15	banjo	18.92	11.32	11.18	6.22	6.29
16	baseball	7.21	18.38	23.41	27.91	27.90
17	basketball	0.00	0.01	0.00	0.00	0.00
18	bathing cap	2.38	4.89	2.44	1.40	1.48
19	beaker	4.17	10.02	10.83	11.70	11.20
20	bear	31.87	29.54	31.77	28.81	29.42
21	bee	12.85	15.61	15.85	14.04	19.51
22	bell pepper	9.21	11.48	7.92	8.84	8.71
23	bench	1.82	3.26	1.07	0.52	0.59
24	bicycle	19.05	21.71	21.87	22.05	21.43
25	binder	3.83	3.31	4.28	4.38	4.90
26	bird	39.59	43.81	47.81	47.24	46.97
27	bookshelf	4.92	7.76	9.55	7.62	7.68
28	bow	0.89	1.10	1.79	1.24	1.20
29	bow tie	0.23	0.12	0.10	1.88	1.49
30	bowl	5.08	5.37	6.29	8.40	7.58
31	brassiere	9.01	10.68	11.26	11.18	11.67
32	burrito	3.03	2.16	5.01	5.00	5.33
33	bus	28.70	37.36	36.12	36.26	34.82
34	butterfly	60.85	60.18	67.47	67.87	67.47
35	camel	6.66	7.92	9.59	10.65	10.33
36	can opener	8.48	11.41	12.15	10.64	12.79
37	car	21.11	22.33	22.98	24.82	25.07
38	cart	12.62	11.46	11.52	11.68	11.01
39	cattle	9.97	3.35	6.24	5.39	6.27
40	cello	6.49	12.75	13.70	16.99	16.92
41	centipede	13.34	12.75	16.59	16.26	19.86
42	chain saw	0.09	0.70	2.08	1.80	2.17
43	chair	4.03	5.13	6.10	5.60	5.53
44	chime	6.94	10.43	7.81	3.31	6.34
45	cocktail shaker	11.75	10.23	13.56	14.93	15.37
46	coffee maker	3.31	12.70	12.36	15.27	11.37
47	computer keyboard	3.18	5.89	9.20	11.36	11.78
48	computer mouse	1.70	1.71	1.71	2.78	2.21
49	corkscrew	13.03	9.63	10.76	13.17	13.06
50	cream	3.06	5.61	6.80	10.82	10.65

TABLE I: Per-class AP on the ILSVRC13 detection *val2*.

#	Category	W0	W1	W2	W3	W4
51	croquet ball	1.72	0.66	0.28	0.16	0.25
52	crutch	1.34	1.96	1.79	1.85	2.78
53	cucumber	5.22	4.52	3.59	3.65	3.41
54	cup or mug	7.51	7.28	11.99	12.10	12.67
55	diaper	1.46	4.60	3.13	3.43	2.96
56	digital clock	4.62	13.05	20.51	19.04	19.35
57	dishwasher	7.79	0.79	0.96	0.70	0.67
58	dog	16.80	15.59	17.34	19.32	17.35
59	domestic cat	4.10	3.87	3.15	4.87	3.23
60	dragonfly	18.44	16.02	26.51	25.22	25.29
61	drum	0.23	0.42	0.57	0.56	0.57
62	dumbbell	2.56	1.49	1.43	1.32	1.36
63	electric fan	28.65	16.71	16.83	20.57	21.10
64	elephant	31.17	38.46	34.92	37.21	34.44
65	face powder	9.96	7.85	6.27	5.19	4.65
66	fig	7.56	7.69	6.70	4.59	4.10
67	filming cabinet	3.60	6.26	7.72	6.92	7.74
68	flower pot	0.24	0.39	0.28	0.27	0.27
69	flute	0.08	1.68	1.67	1.60	1.57
70	fox	22.61	28.19	28.73	32.96	36.23
71	french horn	9.17	10.71	10.50	16.79	12.28
72	frog	22.53	28.31	29.88	29.37	30.08
73	frying pan	5.08	4.03	4.41	5.79	5.70
74	giant panda	34.60	46.05	46.31	26.62	26.71
75	goldfish	5.37	9.75	7.69	9.40	9.42
76	golf ball	17.15	22.84	23.18	23.10	22.91
77	golfcart	32.61	24.31	28.82	31.24	33.59
78	guacamole	13.27	8.80	8.33	8.65	8.28
79	guitar	5.49	5.35	6.69	4.91	4.82
80	hair dryer	3.74	0.44	0.86	1.36	1.28
81	hair spray	1.71	2.57	3.85	3.75	4.94
82	hamburger	15.57	31.05	25.96	17.97	17.92
83	hammer	0.72	0.54	0.64	1.27	1.58
84	hamster	41.87	31.78	42.78	39.35	39.29
85	harmonica	0.49	0.94	0.76	0.62	0.50
86	harp	21.65	30.85	34.71	38.22	37.95
87	hat with a wide brim	6.10	10.00	11.51	9.85	11.37
88	head cabbage	4.92	8.11	8.76	9.63	9.64
89	helmet	5.08	4.10	4.51	5.16	5.43
90	hippopotamus	21.24	24.43	30.54	27.03	27.58
91	horizontal bar	0.04	0.07	0.07	0.05	0.05
92	horse	7.34	6.74	9.30	9.06	8.90
93	hotdog	4.06	4.74	4.12	4.13	3.77
94	iPod	15.80	26.91	26.39	25.08	25.70
95	isopod	10.06	13.45	12.88	13.31	10.11
96	jellyfish	7.32	3.41	2.76	4.39	4.36
97	koala bear	37.38	46.53	50.72	56.96	52.95
98	ladle	0.47	1.75	0.52	0.57	0.58
99	ladybug	11.74	13.94	13.06	13.69	13.35
100	lamp	0.99	0.87	0.61	0.53	0.58

#	Category	W0	W1	W2	W3	W4
101	laptop	7.60	14.38	15.47	18.66	18.75
102	lemon	5.81	10.57	14.28	14.60	15.03
103	lion	4.51	0.80	2.56	2.04	1.90
104	lipstick	3.50	3.74	3.14	4.04	3.85
105	lizard	6.39	11.37	13.14	13.30	13.78
106	lobster	5.12	8.48	17.80	19.80	15.46
107	maillot	0.20	1.64	1.35	1.05	1.36
108	maraca	3.36	2.65	1.53	1.57	1.55
109	microphone	0.07	0.03	0.06	0.10	0.11
110	microwave	19.30	18.18	14.61	14.25	14.32
111	milk can	16.62	19.41	21.39	14.75	17.97
112	miniskirt	0.74	0.89	0.48	0.19	0.20
113	monkey	17.49	18.81	24.26	26.50	24.46
114	motorcycle	19.21	19.08	26.79	26.96	26.70
115	mushroom	13.53	16.11	17.66	18.54	18.66
116	nail	0.07	0.44	0.21	0.13	0.19
117	neck brace	0.11	6.26	1.29	0.21	0.20
118	oboe	1.51	7.16	7.52	7.47	7.51
119	orange	3.85	1.69	5.58	6.42	6.14
120	otter	2.73	2.19	5.89	8.51	9.02
121	pencil box	2.89	6.76	6.25	4.28	4.84
122	pencil sharpener	1.49	2.35	2.05	1.42	1.59
123	perfume	11.55	2.33	5.54	5.09	5.48
124	person	0.14	0.27	0.37	0.47	0.47
125	piano	5.06	3.21	9.26	11.43	11.45
126	pineapple	6.20	12.69	12.49	11.82	11.92
127	ping-pong ball	0.01	0.01	0.01	0.01	0.01
128	pitcher	3.66	5.98	7.53	8.35	8.08
129	pizza	8.89	17.77	14.55	11.71	11.55
130	plastic bag	0.39	2.21	2.74	2.82	2.55
131	plate rack	1.78	1.08	2.62	6.29	6.19
132	pomegranate	8.72	8.89	9.15	9.24	9.42
133	popsicle	0.06	0.04	0.01	0.01	0.01
134	porcupine	24.08	26.20	33.64	29.51	31.30
135	power drill	0.83	1.01	5.40	7.14	7.10
136	pretzel	3.33	4.79	6.04	6.20	6.40
137	printer	6.17	2.79	2.37	2.42	2.29
138	puck	0.01	0.01	0.01	0.01	0.01
139	punching bag	0.58	2.33	3.65	4.35	4.03
140	purse	0.82	1.23	1.32	1.28	1.29
141	rabbit	43.34	48.27	47.09	48.31	48.41
142	racket	0.05	0.06	0.08	0.08	0.06
143	ray	10.26	14.08	19.76	20.22	22.67
144	red panda	16.13	27.36	22.34	25.36	25.28
145	refrigerator	9.90	10.05	8.14	9.21	8.13
146	remote control	17.05	26.71	32.35	24.36	25.56
147	rubber eraser	0.01	0.01	0.01	0.01	0.01
148	rugby ball	0.04	0.06	0.05	0.04	0.04
149	ruler	0.30	1.89	3.84	3.66	3.90
150	salt or pepper shaker	9.99	8.50	7.69	5.45	6.92

#	Category	W0	W1	W2	W3	W4
151	saxophone	15.90	14.08	13.23	11.66	12.78
152	scorpion	15.23	17.18	22.04	18.47	16.83
153	screwdriver	0.11	0.17	0.13	0.68	0.35
154	seal	2.22	3.18	3.33	3.30	3.96
155	sheep	18.81	14.57	18.88	19.25	18.59
156	ski	0.09	0.02	0.14	0.06	0.06
157	skunk	6.61	9.70	9.19	12.30	10.85
158	snail	24.51	11.68	16.11	19.22	19.46
159	snake	1.58	5.20	12.69	15.81	16.05
160	snowmobile	21.22	31.10	27.13	25.74	28.05
161	snowplow	33.11	38.49	37.20	41.74	41.12
162	soap dispenser	0.01	0.50	0.19	0.20	0.17
163	soccer ball	20.17	19.04	17.84	18.06	18.04
164	sofa	7.65	8.22	7.14	7.66	7.71
165	spatula	0.04	0.04	0.07	0.11	0.12
166	squirrel	17.91	10.72	16.12	25.52	23.18
167	starfish	3.88	9.89	13.17	17.33	17.25
168	stethoscope	2.12	2.97	7.39	7.67	7.74
169	stove	0.58	1.32	1.81	2.18	2.04
170	strainer	0.14	0.26	0.87	3.64	3.76
171	strawberry	4.90	7.82	7.52	7.33	7.20
172	stretcher	0.10	0.01	0.15	0.10	0.10
173	sunglasses	1.51	2.52	1.39	1.35	1.74
174	swimming trunks	0.11	0.03	0.00	0.00	0.00
175	swine	18.70	23.02	28.07	34.95	31.21
176	syringe	1.55	2.62	2.64	2.64	2.62
177	table	1.36	3.18	3.77	3.25	3.34
178	tape player	11.73	8.12	8.94	9.92	10.32
179	tennis ball	8.88	7.11	1.61	1.75	1.35
180	tick	19.72	18.95	24.49	17.99	18.74
181	tie	3.13	2.91	3.43	2.25	3.28
182	tiger	10.38	15.88	18.89	20.83	26.02
183	toaster	22.46	22.21	21.94	21.79	22.69
184	traffic light	1.20	1.14	1.03	0.82	0.90
185	train	10.28	22.47	19.73	17.29	17.68
186	trombone	3.49	4.04	1.15	1.72	1.66
187	trumpet	2.66	4.12	3.75	3.83	3.88
188	turtle	22.47	27.24	31.95	31.68	32.04
189	tv or monitor	20.12	29.23	33.18	33.81	33.84
190	unicycle	0.96	1.51	0.70	0.54	0.56
191	vacuum	1.49	0.50	0.48	0.67	0.37
192	violin	2.02	2.06	3.19	2.42	5.22
193	volleyball	0.02	0.09	0.02	0.02	0.02
194	waffle iron	2.71	2.03	2.29	2.98	4.09
195	washer	41.19	35.88	34.47	30.45	31.32
196	water bottle	5.28	7.32	4.89	6.23	6.05
197	watercraft	6.62	6.55	5.68	3.65	4.39
198	whale	23.15	27.97	32.27	33.57	37.38
199	wine bottle	2.74	1.75	1.87	1.34	1.74
200	zebra	31.42	42.00	43.26	40.14	42.17
—	mAP	9.54	10.88	11.87	12.01	12.13